Physics – Uspekhi **64** (12) 1214 – 1237 (2021)

REVIEWS OF TOPICAL PROBLEMS

PACS numbers: 07.85.Fv, **21.10. – k**, **41.60. – m**

50th ANNIVERSARY OF THE INSTITUTE FOR NUCLEAR RESEARCH, RAS

Nuclear photonics: results and prospects

V G Nedorezov, S G Rykovanov, A B Savel'ev

DOI: https://doi.org/10.3367/UFNe.2021.03.038960

Contents

Abstract. We review the modern state of research in a new scientific field that has emerged recently: nuclear photonics. The name is primarily associated with the development of new-generation gamma-ray sources based on traditional and laser–plasma electron accelerators. The use of the Compton backscattering method to ensure the required parameters of gamma-ray beams provides a high energy and high intensity of the beam, low angular divergence, and a high degree of polarization. Beams of ions, neutrons, and other particles can also be formed using modern high-power laser systems. Overall, the sources produced allow solving a number of important fundamental and applied problems, including optical anisotropy effects in nuclei and studies of nonlinear quantum electrodynamic effects in strong electromagnetic fields and of the excitation of nuclear isomers. Among the important applied problems are the generation of neutrons and positrons, laboratory astrophysics, the development of nuclear nonproliferation inspection systems, and nuclear medicine and biology.

Keywords: nuclear photonics, Compton scattering, gamma-ray sources, nuclear spectroscopy

V G Nedorezov [1,a], **S G Rykovanov** [2,b], **A B Savel'ev** [3,4,c]
[1] Institute for Nuclear Research, Russian Academy of Sciences, prosp. 60-letiya Oktyabrya 7a, 117312 Moscow, Russian Federation
[2] Skolkovo Institute of Science and Technology, Bol'shoi bul'var 30, str. 1, 121205 Moscow, Russian Federation
[3] Lomonosov Moscow State University, Department of Physics, Leninskie gory 1, str. 2, 119991 Moscow, Russian Federation
[4] Lebedev Physical Institute, Russian Academy of Sciences, Leninskii prosp. 53, 119991 Moscow, Russian Federation
E-mail: [a] vladimir@cpc.inr.ac.ru, [b] S.Rykovanov@skoltech.ru, [c] abst@physics.msu.ru

Received 16 September 2020, revised 19 March 2021
Uspekhi Fizicheskikh Nauk **191** (12) 1281 – 1306 (2021)
Translated by S Alekseev

1. Introduction

The development of laser methods for producing relativistic particles with energies above nuclear reaction thresholds has given rise to a new research field, nuclear photonics. This term does not yet have a clear-cut definition, because it combines a range of various interdisciplinary fields.

No monographs or reviews on nuclear photonics are available as yet, the reason being that this discipline has formed only very recently. However, we can refer, for example, to the proceedings of a conference on nuclear photonics [1], whose program covered the following areas: Compton gamma sources and related acceleration technologies, ultra-high-power lasers and related technologies, precision photonuclear spectroscopy, isotope separation, photoexcitation of isomers, photofission and nuclear transmutations, ultrarelativistic laser interactions and quantum electrodynamics effects, production and study of rare isotopes, photonuclear cosmology, gamma monochromators, gamma optics and detectors, generation of positrons,

neutrons, electrons, protons, and other particles, industrial safety, and medical applications.

Photon beams obtained by various methods are used in so many different areas that it is practically impossible to discuss them in a single review. The term 'nuclear photonics' appears to have been first used in [2] in 2012. It was then used in 2014 at a conference on nuclear safety and nuclear nonproliferation in Japan [3]. Since 2016, ''Nuclear Photonics'' conferences have become regular and are held every two years. This research field has an extremely high potential for innovations. One of the conference organizers [1, 3], Dr. Chris Barty from the Livermore National Laboratory, USA, noted that, in 2016, investments in this area amounted to several billion US dollars.

We begin this review by discussing the principal mechanisms of particle acceleration in laser plasmas. We describe installations at which laser beams of high peak power are used to produce beams of relativistic electrons, fast ions, positrons, neutrons, and gamma quanta.

Section 3 is devoted to the study of nonlinear quantum electrodynamics effects in the interaction of laser radiation with electrons, including in Compton scattering.

In Section 4, we consider some general laws of photoabsorption of nuclei depending on the photon energy. It should be borne in mind here that research in nuclear photonics can relate to diverse nuclear physics problems, such as electromagnetic interactions of relativistic ions and Coulomb dissociation. Extending this review to these subjects would increase its size and raise a number of debatable problems, because there is still no consent in the world literature on the description of these physical processes. We therefore limited ourselves to the discussion of photonuclear reactions only. We specifically focus on problems that are now being studied at a new level with the use of new-generation gamma beams.

In Section 5, we describe some applied and interdisciplinary fields related to the use of new-generation gamma sources, including astrophysics, gamma tomography of large-capacity containers, biology, and medicine.

In Section 6, we draw our conclusions on the prospects for a new scientific field, nuclear photonics.

2. Laser–plasma particle accelerators

2.1 High-power femtosecond laser systems

For charged particles to be accelerated by a laser field to subluminal velocities, a laser radiation intensity is needed that exceeds the so-called relativistic one

$$I_{\mathrm{R}} = \frac{1380}{\lambda^2} \tag{1}$$

(wavelength λ is expressed in micrometers, and intensity, in PW cm^{-2}), which corresponds to an electromagnetic field with the normalized vector potential $\mathbf{a} = e\mathbf{A}/mc = 1$ (where e and m are the electron charge and mass). In what follows, we use a_0 to denote the amplitude of the vector potential $\mathbf{a}$.

Increasing the laser radiation intensity requires using the shortest possible laser pulses. For the development of approaches that ensured the amplification of ultrashort pulses to high energies and hence the production of ultrastrong fields, G Mourou and D Strickland were awarded the Nobel Prize in Physics in 2018 [4]. Presently, the duration of 25 fs has been achieved for pulses carrying significant energy.[1] The relativistic regime of the interaction of laser radiation with matter was recently realized for extremely short, 7 to 8 fs, laser pulses with a peak power of about 1 TW in the extremely tight focusing regime [5]; however, the possibility of using installations of this type for nuclear photonics studies has to be discussed separately. We also note that focusing a light beam onto a spot with a diameter of the order of the wavelength (to maximize the intensity) is undesirable, because this significantly increases the divergence and the width of the energy spectrum of particles.

An increase in the peak and average flux of accelerated particles is associated with an increase in the energy and repetition rate of laser pulses: the total number of particles accelerated per pulse is proportional to the laser pulse energy, and the pulse repetition rate determines the average current of accelerated particles. For high-power femtosecond laser systems, this frequency is steadily increasing due to progress in laser technologies: the introduction of diode pumping, the search for optimal configurations of amplifying stages, cooling circuits, etc.

For nuclear photonics, both 'desktop' femtosecond lasers, which can be installed in conventional research laboratories, and ultra-high-power laser complexes, often located inside dedicated structures, are of major interest. The first type of laser is characterized by a peak radiation power P up to 10 to 30 TW at the pulse repetition rate $f = 10-50$ Hz (and 1–10 kHz in the near future [6]). Such lasers are currently operating in hundreds of laboratories around the world, but even such facilities are rather scarce in the Russian Federation. Only the installation at Lomonosov Moscow State University is used for research on the subject of our interest here, but its peak power is insufficient (1 TW, 10 Hz) [7]. A number of experiments were carried out at the Central Research Institute of Mechanical Engineering (TsNIIMash) [8] and at the Russian Federal Nuclear Center, the Zababakhin National Research Institute of Technical Physics (RFNC–VNIITF) [9] at facilities with a peak power of 10 TW; however, the operating mode of these lasers (single pulses 1 ps in duration) does not define them as a promising research facility.

There are a number of installations with an 'intermediate' peak power of 50–200 TW and a pulse repetition rate up to 10 Hz, which are produced by commercial companies on demand or are created 'in-house' by scientific groups. In the Russian Federation, the only laser complex of this kind on which work is carried out on the subject under discussion here is the RFNC–VNIITF 100 TW laser [10].

The second type of laser is unique scientific installations whose peak power currently reaches 10 PW at a repetition rate up to 1 Hz. They are produced in the framework of special research programs and collaborations. An overview of the current state of affairs in this area and development prospects is available in [6, 11]. In this review, the pan-European project ELI (Extreme Light Infrastructure) deserves special mention: it unites three newly created scientific complexes located in the Czech Republic, Romania, and Hungary [12] and is aimed at ion acceleration, biomedicine, and laboratory astrophysics (ELI Beamlines,

[1] Recent paper [312] reports the use of postcompression for producing pulses 11 fs in duration with a peak energy of 1.5 PW, which opens up new prospects for the acceleration of charged particles and for studies in nuclear photonics.

Czech Republic [13]), laser-induced nuclear physics (ELI-NP, Romania [14]), and the dynamics of ions, atoms, molecules, and electrons in solids on femto- and attosecond scales (ELI-Alps, Hungary [15]). The main research facilities of ELI-NP are two 10 PW lasers (25 fs, 0.1 Hz) with an on-target peak intensity over 10^{23} W cm^{-2}, as well as a synchronized Compton laser source based on a linear accelerator and a nanosecond laser. A high-power high-frequency laser under construction at ELI-Alps is regarded as a test ground for advancing nuclear waste decontamination technologies.

The Russian Federation has the only PEARL laser complex (0.5 PW, single-pulse mode), created and operated by the Institute of Applied Physics (IAP, Russian Academy of Sciences, Nizhny Novgorod) [16]; in addition, the XCELS project is in the development stage [17], whose implementation would provide the creation of a laser complex with a record total peak power $P \sim 200$ PW.

The typical average power of petawatt laser systems already in operation and under construction does not exceed hundreds of watts. An increase in the average power can be achieved in the framework of the ICAN concept [18], via coherent parallel amplification of an initial femtosecond pulse in a large number of active optical fibers to a subpetawatt peak power, with a mean power of tens of kilowatts.

2.2 Laser–plasma electron accelerators

The key idea of the possibility of accelerating electrons to relativistic energies in a rarefied plasma by an intense laser pulse was first discussed in [19] and is called LWFA (laser wake field acceleration); modern setups of such acceleration in the plasma bubble regime are underlain by computational work [20] and experiments performed a little later [21–23]. The processes occurring during laser acceleration of electrons are described in detail in reviews [24–27].

When an ultrashort relativistic laser pulse propagates in plasma, the ponderomotive force $F_\mathrm{p} \propto \nabla E^2$ pushes electrons in the radial direction, thereby forming a plasma cavity (or a channel, Fig. 1) at the trailing edge of the pulse. The longitudinal electric field

$$E_\parallel = \frac{mc\omega_\mathrm{p}}{e}\,\frac{a_0^2/2}{\sqrt{1+a_0^2/2}} \qquad (2)$$

appears inside the cavity (where ω_p is the plasma frequency). Typical spatial field strength distributions for the longitudinal and transverse quasistationary electric fields are shown in Fig. 2. The longitudinal field accelerates electrons and the transverse field focuses them onto the axis. The longitudinal field strength is 10 GV cm^{-1} for $a_0 \sim 1$, which significantly exceeds the typical values attainable in traditional particle accelerators (up to 50 MV m^{-1}). Various approaches have been implemented for the injection of accelerated electrons [25]: injection upon wake wave breaking, ionization injection, injection using an auxiliary laser pulse, injection of an external electron bunch, and so on.

The maximum energy that can be imparted to an electron during acceleration in the LWFA regime is determined by, besides the actual magnitude of the accelerating field (2), the length on which this acceleration occurs. The following key factors limiting that length can be distinguished: energy depletion and a change in the shape of the laser pulse, laser beam divergence, and dephasing of the accelerated electron pulse with respect to the laser pulse [24, 25]. The maximum

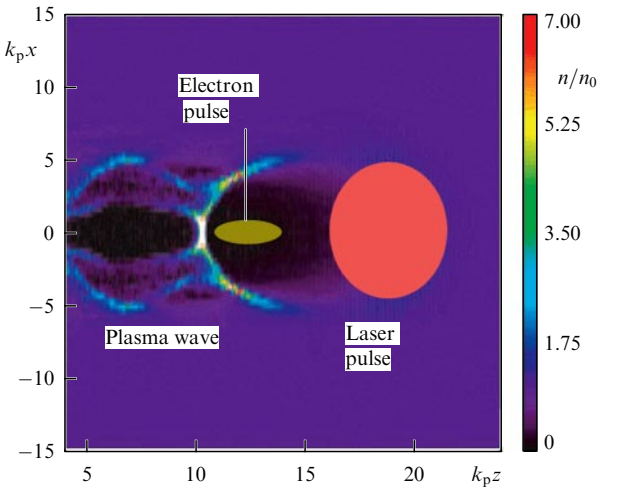

Figure 1. Plasma wave excited by a laser pulse with $a_0 = 5$, propagating from left to right in a plasma with initial concentration $n_0 = 7 \times 10^{18}$ cm^{-3} [26].

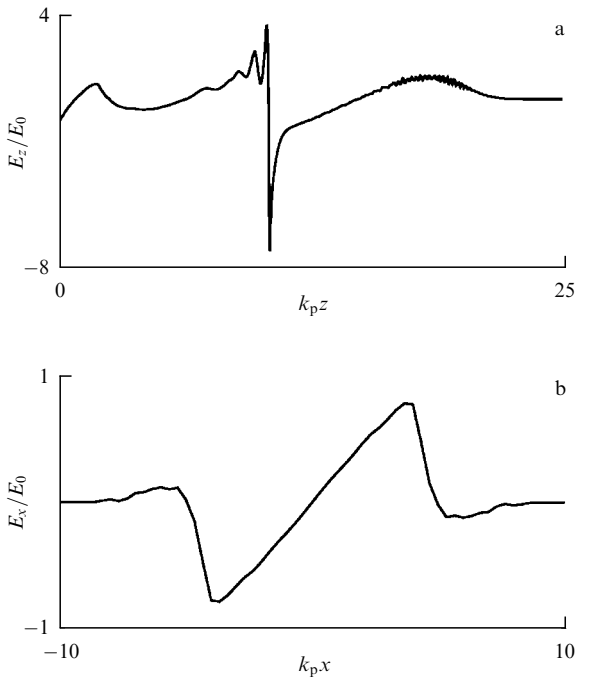

Figure 2. Spatial distributions (a) of a longitudinal electric field on axis $E_z(x = 0)$ and transverse electric field E_x with $k_\mathrm{p}z = 13$, and (b) of a quasistatic electric field corresponding to Fig. 1 [26].

energy [28]

$$W_\mathrm{max} \approx 0.26\left(\frac{P}{\lambda^4 n_\mathrm{e}^2}\right)^{1/3} \qquad (3)$$

is ~ 1 GeV at $a_0 = 2$, $n_\mathrm{e} = 1$, and $\lambda = 0.8$ (in (3), energy is expressed in GeV, λ in micrometers, and peak power P in TW, and concentration of electrons n_e is normalized to 10^{18} cm^{-3}).

The characteristics of an accelerated electron beam substantially depend on the relation between the laser pulse duration and the initial electron concentration [24, 25]. For a number of problems in nuclear photonics, electron beams with a quasiexponential spectrum and large divergence obtained in the LWFA regime [24] are of significant interest

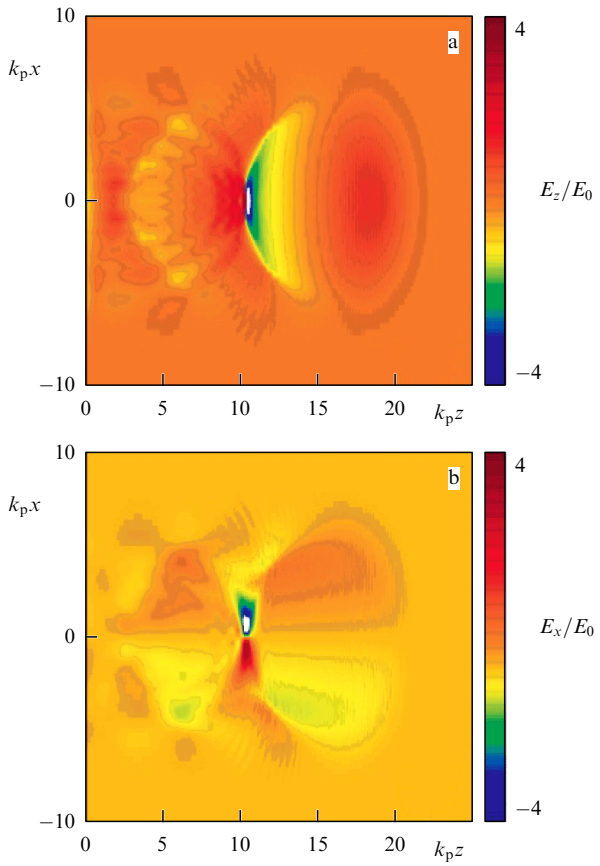

Figure 3. Spatial distributions of the longitudinal, E_z (a), and transverse, E_x (b), fields in a plasma wave in the plasma bubble mode at $a_0 = 0.5$ [26].

due to the large charge of the electron bunch and the relative simplicity of experimental implementation.

Under certain conditions, a laser pulse propagation regime is possible, such that a single cavity with a nearly spherical shape, the so-called plasma bubble (or blowout regime, Fig. 3), forms at the trailing edge of the pulse. It is in this regime that electron bunches with a small energy spread and low emittance are formed. In pioneering studies [21–23], electron bunches with a charge up to 0.5 nC, an average energy of about 80–90 MeV at the energy spread of several MeV, and a normalized beam emittance of ~ 3 mm mrad were obtained in the irradiation of dense helium jets with laser pulses. Importantly, such a beam was obtained with an acceleration length of only a few millimeters.

An increase in the acceleration length (and the electron energy) is achieved by a simultaneous decrease in the electron concentration and an increase in the laser pulse energy while preserving its intensity. In [29–31], electron bunches with an average energy of 3–4 GeV were obtained using installations with a subpetawatt peak laser power. The maximum acceleration up to 7.8 GeV was achieved using a laser system with the peak power of 0.85 PW [32] with the laser beam channeled into a capillary discharge 20 cm in length. Bunches were obtained with a charge up to 50 pC and angular divergence of 0.2 mrad at an electron beam diameter of less than 100 microns.

We note that a decrease in the duration of laser pulses allows proportionally decreasing the required pulse energy (see (3)) and significantly increasing the optimal electron concentration. In [33], laser pulses with a duration of 3–4 fs and energy of only 2–3 mJ at a repetition rate of 1 kHz were used to obtain electrons with energies of 6–9 MeV in the form of a beam with a divergence of 35 mrad and bunch charge of 0.5 pC in a superdense nitrogen jet ($\sim 0.1 n_c$, where n_c is the critical concentration).

In the Russian Federation, experimental studies on the wake acceleration of electrons are carried out only at the IAP at the PEARL subpetawatt facility. In the experiment in [34], beams of electrons with energies up to 300 MeV were obtained. In [35], it was reported that electrons with energies up to 1 GeV were obtained at the same facility.

The conditions (pertaining to a_0, n_e, etc.) for the formation of the initial electron bunch differ significantly from the optimum conditions of beam acceleration to high energies. In addition, the depletion of the laser pump pulse energy becomes a significant problem. For example, the initial proposal to accelerate an electron bunch to 1 TeV was to use a laser accelerator 29 m in length with a laser pulse energy of 1600 J and a duration of 0.7 ps [36]. The idea of a multistage accelerator seems to be more efficient, allowing independent laser pumping to be used at each stage, with the parameters of the plasma and laser pulse optimized for each of the stages [37–39].

The first calculations of a 0.5-TeV linear laser accelerator were published in [37]. It was shown there that the total length of such an optimized accelerator, with the necessary spacing between the accelerators proper taken into account, would be 200 m, with the number of stages equal to 100. A series of experiments on two-stage acceleration performed so far [39] shows that this technology is at the early stage of its development: the electron energies are significantly lower than the record values obtained with one-stage acceleration. The current European project EuPRAXIA [40] is expected to use multistage laser–plasma acceleration to produce a high-quality electron beam with an electron energy of 5.5 GeV at a 5% energy spread [41]. Modern laser technologies also invite discussions of the acceleration of electrons to energies of hundreds of TeV [42], with the accelerator length being equal to several kilometers and a laser pumping energy of several MJ.

An approach is also under discussion where, after the depletion of laser pumping and/or the dephasing of the electron and laser pulses, the accelerated electron bunch itself forms a wake wave [43–46], which means that a transition to the PWFA (plasma wake field acceleration) regime occurs. A new electron bunch is then injected into the newly formed accelerating structure, which allows accelerating the beam to energies several times higher than the energy of the initial electron bunch. Another novel scheme, which received the abbreviation TWEAC (traveling wave electron accelerator), was proposed in [47]. There, an accelerating plasma structure is formed by two crossed focused beams with oblique phase fronts. This ensures the motion of the accelerating structure at nearly the speed of light and eliminates the electron beam dephasing problem. Calculations show that the TWEAC scheme can provide acceleration to energies of several TeV in a single-stage version. No experimental tests of the scheme have so far been reported.

Another approach to overcoming the limitation due to the dephasing of electrons was discussed in [48]. The proposal there was to use special aberrations introduced into the beam without changing the duration of the ultrashort pulse in order to create a configuration of an electromagnetic field with the intensity maximum, located on the beam axis (and creating a

plasma wave), that moves with any predetermined phase velocity over any distance through the plasma. Calculations have shown that very high energies of the electron beam can be achieved: electrons with an energy of several TeV can be obtained at a distance of 4.5 m. We note that this scheme also eliminates the need for waveguide structures to guide the laser beam. The principal fundamental limitation of the proposed scheme appears to lie in the complexity of manufacturing the nontrivial optical elements necessary for its implementation, especially at high peak laser radiation powers.

The generation of relativistic electrons and powerful fluxes of gamma quanta is also possible when solid targets are irradiated with a laser pulse. This process occurs in two stages: the acceleration of electrons to energies of several to hundreds of MeV in dense subcritical plasma and the generation of gamma quanta in the bulk of the target in inelastic scattering by ions and atoms. Various electron acceleration mechanisms have been identified in this interaction mode: jxB heating [49], direct acceleration in a plasma channel (DLA, direct laser acceleration) [50], stochastic heating [51, 52], parametric instabilities in the region of a quarter of the critical concentration n_c [53, 54], and some others. The role of a specific mechanism depends on a combination of factors: the spatial profile of the subcritical plasma created by prepulses of different natures, and especially its gradient in the region of $0.2-0.5n_c$, and the intensity and duration of the laser pulse. These issues are partly covered in more detail in books [55, 56] and in numerous research papers.

Each of the acceleration mechanisms has its own essential features and results in the characteristics of the electron energy and angle distributions with different dependences on the laser pulse parameters. A typical energy spectrum of electrons is a biexponential distribution with the 'temperature' of the less energetic component given by [57]

$$T_h \approx mc^2 a_0^{2/3}, \tag{4}$$

where by temperature we mean the parameter of the exponential approximation of the electron spectrum $dN_e/dE_e = K\exp(-E_e/T_h)$. The second component can have a much higher temperature, which strongly depends on the specific conditions of the experiment. Nevertheless, just that part of electrons typically have energies that significantly exceed the rest energy, and are responsible for the generation of gamma radiation.

Based on the energy and momentum conservation laws, an estimate common to all interaction modes was obtained in [58] in the form

$$T_h \approx 0.7mc^2 a_0\sqrt{\eta_e}, \tag{5}$$

where

$$\eta_e \approx 5\times 10^{-2} a_0^{3/2} \tag{6}$$

is the proportion of energy transferred to plasma electrons [59], which reaches 50% at $a_0 \sim 5$.

The angular spectrum of electrons here has the divergence measured by fractions of a radian. In some cases, for petawatt [60] and terawatt [61] laser pulses, with a special preparation of the preplasma, electron beams with a divergence one or two orders of magnitude lower can be obtained.

Because the energies of electrons are relatively small (from several to several ten MeV), gamma quanta are emitted into a fairly wide solid angle. But because the efficiency η_e is large and significantly exceeds the corresponding quantity for LWFA, the total radiation dose provided by the resulting source turns out to be high (several mrad per joule of laser energy input [62]).

2.3 Laser acceleration of protons and multiply charged ions

The interaction of superintense laser radiation with dense targets also leads to the acceleration of protons as well as heavier multiply charged ions. A number of previously published reviews [63–67] are devoted to a detailed discussion of these processes.

At moderate intensities, laser radiation interacts with electrons, while ions can be considered immobile during the action of a laser pulse due to their much greater mass. As the 'threshold' intensity $I_{th}^{(i)}$ above which this is no longer the case, we take the intensity at which the energy of oscillations of a relativistic electron in an external electromagnetic field is of the order of the rest energy of an ion with a mass m_i:

$$I_{th}^{(i)}\lambda^2 \approx I_R\lambda^2\frac{m_i}{m}. \tag{7}$$

For the proton, this intensity is 1.6×10^{21} W cm^{-2} ($\lambda = 0.8$ μm). We note that intensities one or two orders of magnitude higher are already expected to be attained in the near future (see Section 2.1).

Obtaining a directed beam of protons with energies above several MeV in relativistic laser–plasma interaction is associated with the use of thin (from several to several ten micrometers) films as a target and with the TNSA (target normal sheath acceleration) mechanism [68]. In this regime, the flow of electrons accelerated forward on the front surface of a thin foil reaches its rear surface and, escaping further into the vacuum, forms a charge separation field (the so-called ambipolar field) (Fig. 4). Atoms are then ionized near the rear surface (by both the electron beam and the ambipolar field) and are subsequently accelerated by the ambipolar field to significant energies. This is especially true of protons, which have the highest charge-to-mass ratio at a low mass. The theory of this effect and numerical simulations are presented in a number of original studies and the already mentioned reviews [63, 64]. We also note study [69], where a simple analytic model is presented and the dependences of the maximum attainable proton energies on the laser radiation intensity and laser pulse duration are obtained.

The energy spectrum of protons in the case of TNSA is also quasiexponential, with the slope

$$T_h \approx Zmc^2\left(\sqrt{1+a_0^2}-1\right) \tag{8}$$

(where Z is the ion charge) and the maximum energy

$$E_{i,max} \approx 2T_h\left(\ln\left(t_p+\sqrt{t_p^2+1}\right)\right)^2, \tag{9}$$

which corresponds to several ponderomotive potentials ($t_p \approx 0.5\omega_{pi}\tau$, where ω_{pi} is the ion plasma frequency).

The TNSA scheme ensures the formation of a proton beam with energies up to tens of MeV at intensities up to 10^{20} W cm^{-2}: in the first studies [70–72], the proton energies

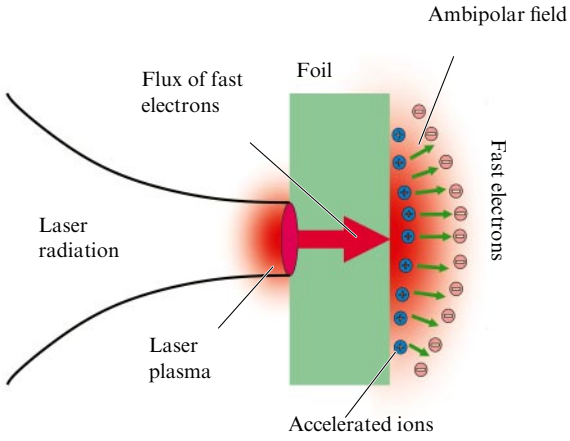

Figure 4. Ion acceleration scheme in the TNSA mechanism.

reached 58 MeV, and later exceeded 85 MeV [73]. The number of particles obtained by acceleration by one laser pulse is in the range of $10^{10}-10^{11}$. It is also worth noting paper [74], where the proton beam coming from a laser plasma was controlled using a plasma lens, also produced by a laser pulse. This opens up interesting prospects for the dynamical control of proton beams accelerated in laser plasma.

In the interaction regime under discussion, ions with a large mass and charge can also be accelerated. In [75], the action of picosecond laser pulses with a peak power of 50 TW (intensity up to 10^{19} W cm^{-2} on a lead target) allowed obtaining both protons with an energy up to 10 MeV and lead ions with the charge $Z = 48^{+}$ and energy up to 5 MeV per nucleon. For a more efficient acceleration of heavy multiply charged ions, the surface has to be cleaned from the layer containing hydrogen, i.e., from water and oil films [76–78].

Obtaining proton beams with a narrow energy spectrum and better collimation requires using targets in which hydrogen atoms are present only in a small region on the reverse side of the target foil [79, 80]. The energy and the number of protons obtained in this way are small. The design of the target composition also allows obtaining quasimonoenergetic beams of carbon ions [79] and even gold [81].

At a laser radiation intensity exceeding 10^{20} W cm^{-2}, a number of new ion acceleration regimes can be realized (see review [63]): radiation pressure acceleration [82], acceleration in a collisionless shock wave [83], and break-out afterburner (BOA) acceleration [84]. The published experimental results are few. In [85], fully ionized carbon ions with energies up to 83 MeV per nucleon (in the BOA mode) were obtained using a laser with a peak radiation power of 250 TW and duration of 500 fs. Laser radiation with approximately the same peak power but with the pulse duration of 35 fs, focused so as to attain an intensity of 10^{21} W cm^{-2}, was used to accelerate iron ions Fe^{24+} to energies of 10 MeV per nucleon [86] in the RPA regime. With a further increase in intensity to 3×10^{21} W cm^{-2} (at the peak power of 1 PW and duration of 32 fs), beams of fully ionized gold ions were detected in [87] with energies up to 25 MeV per nucleon with the total number of ions being 2×10^{11} srad^{-1}.

Among the numerous computational studies, we note recent publication [88], where the interaction of a 2 PW laser pulse with a near-critical plasma of hydrogen and carbon was simulated, with the results demonstrating directed beams of protons with energies up to 350 MeV. Another approach, based on the acceleration of ions by light pressure at intensities above 10^{22} W cm^{-2}, was discussed in [89–91], and conditions for laser acceleration of protons to 1–10 GeV were found. In particular, these approaches will be implemented in the near future in the framework of the ELI project [92].

2.4 Generation of neutrons

One of the key applications of laser-accelerated ions is the generation of directed fluxes of neutrons with energies of several, or several ten, or hundreds of MeV [8, 93–96]. Currently, the flux of obtained neutrons reaches $10^{6}-10^{8}$ per joule of the input energy, i.e., from 10^{6} per pulse for terawatt systems with high laser pulse repetition rates to more than 10^{10} for petawatt systems with low repetition rates. In [97], a flux of 6×10^{17} neutrons cm^{-2} per second with an energy of about 100 MeV was achieved with a pulse duration of less than 100 ps. The neutron beam had a rather poor directivity: the number of neutrons along the axis of the laser beam exceeded the number of neutrons at large angles to the axis by about a factor of two. Deuterons coming from a thin film were accelerated by 200 TW laser radiation of the TRIDENT laser system (with the on-target intensity up to 10^{21} W cm^{-2} and pulse duration of 600 fs), and the neutrons were obtained in the subsequent ^{9}Be(d, n) reaction on a secondary target (the so-called pitcher–catcher scheme). In [98], the special preparation of the target, made of a thin gold foil with a layer of deuterated polyethylene, allowed obtaining a much better collimated neutron beam (with the neutron flux on the axis exceeding the flux at large angles by about a factor of 10), but their flux was an order of magnitude lower.

Most applications require fluxes exceeding 10^{12}–10^{15} neutrons per second, which can be realized using kilohertz laser systems (e.g., in the ICAN project) or petawatt laser systems at a repetition rate of tens of hertz (ELI-NP and others). An important feature of neutron pulses obtained using laser-accelerated ions is their short duration. Of considerable interest are therefore those applications in which the decisive role is played not by the average flux of neutrons per second but by the peak value of this flux. With 10^{10} neutrons per pulse and a neutron pulse duration of 100 ps (determined primarily by the width of the energy spectrum of protons and the distance to the secondary target), the instantaneous neutron flux in the experiment in [97] was 10^{20} per pulse. The number of simultaneously generated neutrons can be increased significantly by so-called spallation: irradiation of a target made of a heavy metal (mercury, tantalum, etc.) with high-energy (hundreds of MeV) protons [4]. Each proton then generates 20 to 30 neutrons, which is why a significant increase in the neutron flux can be achieved. According to modern estimates [99], when protons are accelerated by laser pulses with the intensity of 10^{22} W cm^{-2} or higher (ELI-NP and similar installations), sufficiently intense fluxes of protons with energies of hundreds of MeV and hence peak neutron fluxes up to 10^{24} n s^{-1} cm^{-2} can be obtained. We also note the practically important study [100], where calculations demonstrated the possibility of decelerating a neutron beam and forming a beam of epithermal neutrons (with the energy of about 0.5 eV).

2.5 Generation of positrons

Positron beams with a relatively low energy, less than 10 MeV, are of significant interest for problems in nuclear photonics. Recently, we have witnessed rapid progress in the generation of such positron beams with high-power laser pulses [2, 101].

A scheme with direct irradiation of dense heavy targets [102–104] currently provides a large number (up to 10^{12}) of positrons per laser pulse at the laser pulse energy in the range of 100 to 900 J. The best results have been obtained with the use of relatively long, subpicosecond, laser pulses. We also note that, in this case, the divergence of the positron beam is quite large, although it turns out to be less than when linear electron accelerators are used.

A much lower divergence of the positron beam can be obtained using a scheme with separate stages of the laser–plasma acceleration of electrons and the generation of positrons. Placing the target converter very close to the electron acceleration region ensures a small size of the electron beam and allows the positron beam to be collimated. In [105], a neutral electron–positron plasma with a total of 3×10^7 particles of each type and beam divergence of 5–20 mrad was obtained by using an electron beam accelerated by a powerful laser, with the maximal energy of 600 MeV and angular divergence of 2 mrad (FWHM) with the target converter thickness of the order of 2.5 cm. Similar results were obtained in Ref. [106] at a much lower electron energy of 50 MeV, but a much greater bunch charge, ~ 1 nC.

We note that the results obtained to date using both conventional accelerators and high-power lasers on the generation of positrons with energies less than 10 MeV, especially near their generation threshold ($2m_ec^2$), are far from complete and differ greatly among themselves. Therefore, new experimental and numerical studies are needed to create positron sources with optimal parameters.

Positrons of much lower energies are of considerable interest in applications. An important problem is the generation of electron–positron pairs near the threshold of this reaction, when the energy of electrons and gamma quanta is not much higher than $2m_ec^2$. To obtain such electrons, it seems reasonable to use small-size electron accelerators with energies up to 10 MeV and terawatt lasers. Simulations of positron generation and analyses of the available literature data for electron energies below 10 MeV show that a positron source can be created both on the basis of a LUE-8-type linear accelerator at the Institute for Nuclear Research (INR), Russian Academy of Sciences, and on the basis of the femtosecond laser facility at Moscow State University [107]. With the use of the accelerator, the flux of low-energy positrons (up to several MeV) can reach 10^{10} e^+ s^{-1}, and with the laser, from 10^4 to 10^6 e^+ s^{-1}.

3. Compton backscattering method

The rapid development of nuclear photonics as a separate research field is closely related to the development and use of high-luminosity gamma-ray sources based on the Compton backscattering effect. Compton backscattering is the process of scattering photons by a beam of fast electrons with the aim to convert the energy of a scattered photon into the X-ray and gamma ranges. A fairly complete historical background and a description of the current state of the art in the use of gamma radiation sources based on the linear Compton effect are available in [108–113]. In this review, after mentioning experiments done with laser–plasma accelerators, we therefore focus on the nonlinear Compton effect, which theoretically allows increasing the photon yield by several orders of magnitude while maintaining the main useful properties of the source: the high energy of gamma quanta, the narrow emission line, a high degree of polarization, and small angular divergence and duration.

We note the strong influence of the development of laser technology on Compton sources, with high-power laser systems being used for two major purposes. The first is the creation of extremely compact gamma-radiation sources based on laser–plasma accelerators, and the second is a significant increase in the yield of gamma photons within the standard approach to particle acceleration.

3.1 Compton scattering using laser–plasma accelerators

In [108, 110–112], examples are given of modern installations based on traditional accelerators (summarized in a table in [113]). For completeness, we mention the ELI-NP project under construction in Romania [114], with the projected source of gamma quanta in the energy range of 0.5 to 19.6 MeV, the after-collimation intensity of the order of 8×10^8 photons per second, the relative line width less than 0.5%, and the repetition rate of 100 Hz.

In this section, we discuss the use of laser–plasma accelerators for Compton sources of gamma rays. We note that the quality of electron beams from a laser–plasma accelerator is constantly improving [26], and experiments on the use of beams as secondary emitters for obtaining sources of ultraviolet, X-ray, and gamma radiation are being actively discussed and performed [115].

The first experiments on the use of electrons accelerated in a laser–plasma accelerator for Compton scattering were reported in 2006 [116]. The electrons had a thermal spectrum with a temperature of about 6 MeV, and hence the scattered photons also had a wide spectrum extending to the range of soft X-ray radiation. An interesting experiment was published in 2012 [117], demonstrating a wide spectrum of photons that already reached the range of hard X-ray radiation (up to energies of the order of 200 keV). The researchers proposed an interesting and original way to conduct the experiment. A short powerful laser pulse propagating in a gas target accelerated electrons to energies of the order of 100 MeV. A solid-state target placed in the path of propagation of the laser beam was then ionized by the beam itself and served as a plasma mirror reflecting the laser pulse. The laser radiation was then scattered by electrons accelerated in the plasma by the laser pulse itself. In 2016, experiments based on the same principle (wakefield acceleration and a plasma mirror in the path of a laser pulse) were reported: on a 30-TW laser facility at the University of Austin, Texas (USA) [118] and on a 100-TW laser facility at the Shanghai Institute of Optics and Fine Mechanics (SIOM, China) [119]. In the first of these experimental studies, the production of a quasimonoenergetic (full spectral width at half maximum $\sim 50\%$) beam of scattered photons with a peak photon energy up to ~ 200 keV was demonstrated, and in the second, the spectrum width was $\sim 30\%$ and the peak energy extended to 1.4 MeV, i.e., already reached the gamma range.

A series of studies on linear Compton scattering by laser-accelerated electrons was carried out at the University of Lincoln in Nebraska (USA) at a 100-TW Diocles laser facility [120–122]. In [120], the possibility of generating gamma radiation by scattering a laser pulse by electrons accelerated in a wake wave was experimentally demonstrated for the first time: the scattered photon energy reached 4 MeV, although the spectrum was wide. In one shot, a total of about 2×10^7 photons was obtained in the entire wide spectrum. The dimensionless amplitude of the scattered pulse was $a_0 = 0.4$, which means, strictly speaking, that the

scattering was weakly nonlinear. In subsequent experiments, the same research team succeeded in demonstrating a quasimonoenergetic beam of gamma quanta (spectral width at half maximum $\sim 50\%$) with energies up to 1 MeV [121]. A total of about 1.7×10^6 photons was obtained in one shot, and the scattered laser pulse amplitude was $a_0 = 0.3$. In [122], the second harmonic of a part of the laser pulse from the Diocles system was used for scattering, which allowed obtaining a photon spectrum with the central energy of about 9 MeV, extending to 15 MeV. The total number of photons generated in one shot was estimated as 3×10^5.

The above experiments show that the gamma-ray sources do not yet match the characteristics of modern sources based on standard accelerators, be it in peak energy, spectrum width, or number of scattered photons. In the overwhelming majority of studies, the experimentalists did not attempt to achieve a gamma-ray linewidth less than 30–50%, which would be necessary for such sources to be used in nuclear photonics. Nevertheless, we note the project on the construction of a narrow-band (with a line width less than 2%) gamma source based on a laser–plasma accelerator at the Lawrence Berkeley National Laboratory (USA) [123, 124]. Given the current laser pulse repetition rate of 10 Hz, this projected facility can theoretically be compared in terms of the number of generated gamma photons per second onto a thin radiation line with the well-known HIGS (High Intensity Gamma Source) facility [109], and can even significantly exceed it with further development of the technology of increasing the repetition rate of high-power short laser pulses up to 1 kHz (k-BELLA [125, 126]).

We note the main advantages of using laser-plasma accelerators in constructing sources based on the Compton effect. First, they are compact and cheap, which means they are available to a wide range of researchers. Second, because the duration of electron bunches accelerated in a plasma accelerator is in the femtosecond range, both X-ray and gamma radiation obtained due to Compton scattering also have a short duration in the range of several femtoseconds. Compared to the picosecond duration of radiation at HIGS-type facilities, this adds to the attractiveness of plasma accelerator sources in studies of fast processes.

3.2 Nonlinear Compton scattering

Nonlinearity manifests itself in Compton scattering most strongly at the dimensionless scattered laser pulse amplitudes $a_0 \gtrsim 1$, although it must already be taken into account at lower amplitudes when constructing narrow-band gamma sources [127]. From the standpoint of classical physics, if in the case of linear Compton (Thomson) scattering we completely ignore the influence of the laser pulse itself on the longitudinal component of the electron pulse (i.e., ignore the magnetic component of the Lorentz force or, equivalently, the light pressure), then, in the nonlinear case, light pressure must be taken into account, which leads to effects such as the generation of high-order harmonics and the shift of the main scattering line and its harmonics depending on a_0 [128]. From the classical standpoint, nonlinear Compton (Thomson) scattering is similar to wiggler radiation: the calculation methods and the quantitative results are largely similar [129, 130]. From the standpoint of quantum electrodynamics, nonlinear one-photon Compton scattering [131] is a first-order process in the perturbation theory, but the wave function of the electron is 'dressed' by a strong electromagnetic field and is therefore a solution of the Dirac equation in a plane electromagnetic classical wave. This approach is widely used in quantum electrodynamics problems in strong fields [132, 133].

Nonlinear one-photon Compton scattering is a fairly well-studied process from the classical and quantum standpoints, both in electromagnetic waves with a rectangular envelope (including those with infinite duration) and in bounded laser beams with smooth envelopes [128, 131, 133–149]. In this review, we restrict ourselves to those cases where the dimensionless amplitude of the scattered laser pulse is not too large, of the order of unity. Writing the energy–momentum conservation law in the nonlinear case [131] for the 'head-on' collision of an electron with a plane wave, we can express the energy of a photon scattered on the nth harmonic as

$$\hbar\omega_{\gamma,n} \approx \frac{4\gamma^2 n\hbar\omega_0}{1 + a_0^2/2 + \gamma^2\theta^2 + n\chi}\,, \tag{10}$$

where $\chi = 4\gamma\hbar\omega_0/(mc^2)$, γ is the relativistic Lorentz factor of the electron, $\hbar$ is Planck's constant, ω_0 is the frequency of the incident photon, and θ is the angle between the initial direction of motion of the electron and the direction of motion of the scattered photon. Here, n can be understood as the number of photons absorbed by the electron, which then re-emits only one photon. This expression is written for the linear polarization of the scattered pulse. In deriving (10), it was assumed that the scattered pulse is long (or infinite) and its amplitude a_0 is constant. In this case, we can also write the expression for the number of photons emitted by one electron into the relative linewidth equal to the spectral width of the scattered circularly polarized laser pulse (the 'natural' one, i.e., equal to $1/N_u$, where N_u is the number of periods of the laser field):

$$N_{\gamma,\,\mathrm{natural}} \approx \pi\alpha\frac{a_0^2}{1 + a_0^2}\,, \tag{11}$$

where $\alpha = 1/137$ is the fine structure constant. The following conclusions can be drawn. First, the electron cannot emit more than $\pi\alpha \approx 0.023$ photons into a 'natural' line, because a further increase in a_0 leads to a redistribution of scattered photons over harmonics of the main line. For $a_0 \gg 1$, the spectrum of nonlinear one-photon Compton scattering becomes a synchrotron one, i.e., wide and unsuitable for narrow-band gamma-ray sources. Second, as a_0 increases, the number of photons scattered onto a natural line increases (quadratically for $a_0 \ll 1$) and saturates at the dimensionless electromagnetic wave amplitude $a_0 \sim 2$. This means that, to create higher-luminosity sources of narrow-band gamma radiation, it is reasonable to increase the dimensionless quantity a_0 to values of the order of unity or two. Unfortunately, the presented formulas are valid for laser pulses with a rectangular envelope; the creation of such pulses with a large amplitude a_0 is extremely difficult and has not yet been demonstrated. For laser pulses with a smooth (for example, Gaussian) envelope, the situation changes dramatically, as we show in what follows.

We mention the experimental work on nonlinear Compton scattering that was carried out in standard accelerators. In 1983 [150], the generation of the second harmonic in nonlinear Compton scattering was demonstrated for the first time, and a laser pulse with the small amplitude $a_0 = 0.01$ was scattered by an electron beam with an energy of about 1 keV.

Subsequently, the generation of the second harmonic in Compton scattering was also observed at higher amplitudes of the scattered laser pulse in [151] ($a_0 = 0.35$), [152] ($a_0 = 0.7$), and [153] ($a_0 = 1$) when the pulse of a CO_2 laser was scattered on an electron beam with an energy of about 60 MeV. In [154], nonlinear effects were demonstrated in the Compton scattering by electrons in plasma. In study [155], carried out at the Stanford Linear Accelerator Center (SLAC, USA), the simultaneous interaction of up to four laser photons with electrons from a beam with a central energy of 46.6 GeV was demonstrated. The dimensionless laser pulse amplitude (with the wavelength of 1054 nm at the fundamental frequency and 527 nm at the second harmonic) reached $a_0 = 0.6$, and only the electron spectrum was measured.

It is worth mentioning that, at present, due to the simplicity and convenience of synchronization, most of the experimental work on nonlinear Compton scattering is carried out using electrons from laser–plasma accelerators. In [156, 157], the first experiments to measure the effect of nonlinearity in Compton scattering by electrons accelerated in a plasma are mentioned; the dimensionless amplitude was $a_0 = 2$ in [156] and $a_0 = 0.9$ in [157]. We note that, in the first of these studies, the spectrum of scattered photons was wide and extended to 18 MeV, and in the second one, measurements in the X-ray range were presented, with a quasimonoenergetic photon spectrum. In [157], the dependence of the energy of scattered photons on a_0 and the generation of the second harmonic were also demonstrated. In [158, 159], scattering laser pulses with $a_0 \sim 10$ were used, and a wide spectrum of photons extended to tens of MeV. We note the angular dependence of the photon spectrum on a_0 ($\sigma_{\theta,\gamma} \propto (1 + a_0^2/2)^{1/2}/\gamma$), which can be used to determine the a_0 value from experiment. In all studies on nonlinear Compton scattering, the possibility of increasing the luminosity of Compton sources with increasing a_0 is actively discussed and demonstrated.

At the moment, no sources of X-ray or gamma radiation based on nonlinear Compton scattering are available that could be systematically and actively used as centers of collective use, although nonlinear effects must, of course, be taken into account when creating narrow-band sources, especially with the relative linewidth of less than one percent [160].

3.3 Ponderomotive broadening and interference of the nonlinear Compton scattering spectrum

As we have noted, the presence of a smooth (for example, Gaussian) envelope of high-power laser pulses leads to a dramatic difference from the case of a rectangular envelope. Equation (10) for the energy of a scattered photon is written for a laser pulse with a rectangular (or infinite) envelope with a dimensionless amplitude a_0. In the case of a smooth envelope in Eqn (10), the scattered frequency $\omega_{\gamma,n}$ depends on the instant (the instantaneous value of the laser pulse amplitude) at which the scattering event occurs. In the language of classical electrodynamics, the force of light pressure acting on the electron is inhomogeneous and depends on the current value of the electric field: the electron feels the light pressure and 'decelerates' (in the laboratory frame of reference) more strongly at the center of the laser pulse, where the amplitude is higher, than at the edges. This leads to the so-called ponderomotive broadening of the scattering line and its harmonics: when a laser pulse with a smooth envelope is scattered by a relativistic electron, the spectrum of the nth harmonic scattered strictly backwards extends from $4\gamma^2 n\hbar\omega_0/(1+a_0^2/2+n\chi)$ to $4\gamma^2 n\hbar\omega_0/(1+n\chi)$. Thus, the radiation spectrum (of the fundamental line of each harmonic) in the case of nonlinear Compton scattering of a laser pulse with a smooth envelope is not a narrow-band one, but has a relative width $\sim a_0^2/2$ in the case of linear and $\sim a_0^2$ in the case of circular polarization of the scattered pulse.

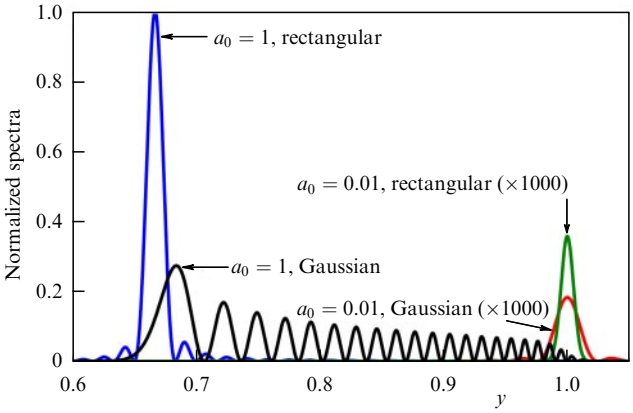

Figure 5. (Color online.) Compton backscattering spectra (at scattering angle π) as functions of dimensionless energy $y = \omega_\gamma/(4\gamma^2\omega_0)$ for laser pulses with different envelopes (rectangular: $a_0 = 1$, blue, and $a_0 = 0.01$, green; Gaussian: $a_0 = 1$, black, and $a_0 = 0.01$, red). All spectra are normalized to the peak value of the on-axis spectrum for the rectangular envelope with $a_0 = 1$.

As an illustration of the effect of ponderomotive broadening of the scattering line, in Fig. 5, we show the spectra of radiation scattered strictly backwards for linearly polarized laser pulses with different envelopes (rectangular and Gaussian) and different amplitudes ($a_0 = 0.01$ and $a_0 = 1$). The parameters are chosen such that the total energy of a pulse with a rectangular envelope is equal to the total energy of a Gaussian pulse with the same amplitude. In Fig. 5, for a Gaussian pulse with amplitude $a_0 = 1$ (black line), in addition to the ponderomotive line broadening, we also see interference in the spectrum of the main scattering line. This is a consequence of the fact that, for a laser pulse with a smooth envelope, the probability of obtaining a photon with a certain energy after the scattering event can have a sharp maximum twice per pulse: once at an increasing intensity and once at a decreasing one. When calculating the scattering matrix, these two possible scattering events enter the calculation with their phases depending on the particle position; therefore, for different energies of scattered photons, both constructive and destructive interference in the scattering spectrum is possible [136, 141].

Ponderomotive broadening of the scattering line is a well-known problem in nonlinear Compton scattering of pulses with a smooth envelope; it is one of the main reasons why there are no experiments demonstrating narrow-band sources (with a relative width $< 10\%$) for scattered laser pulses with $a_0 \sim 1$. All the existing sources for nuclear photonics currently operate in the linear regime, although weakly nonlinear effects are taken into account [160].

3.4 Methods for combating ponderomotive broadening

A natural question arises as to whether any methods for combating parasitic ponderomotive broadening are available in addition to the generation of laser pulses with a rectangular envelope.

In 2013, a numerical example was used in [161] to propose the original and interesting idea of the nonlinear chirping of a laser pulse for 'tuning' the local frequency of the pulse to the local frequency of the scattered photon. This idea was subsequently developed in detail analytically and numerically in several studies, in both classical [148, 162–165] and quantum [166] formulations. Let the laser pulse propagate along the z-axis, and let $g(\eta)$ be the envelope of the vector potential of the linearly polarized pulse, normalized to unity. In this case, with the properly chosen instantaneous frequency of the pulse

$$\omega_{\mathrm{L,\,chirp}}(\eta) = \omega_0\left(1 + \frac{a_0^2}{2}\, g^2(\eta)\right),$$

where $\eta = \omega_0 t - (\omega_0/c)z$, in the scattering of such a laser pulse with an arbitrarily large amplitude a_0 by an electron (within the applicability of the one-photon approximation and in the absence of the radiation friction force [148]), the spectrum of scattered photons is narrow-band. It follows from the expression for $\omega_{\mathrm{L,\,chirp}}$ that the experimental implementation of the idea of nonlinear chirping requires laser systems with a very wide spectrum: for example, for $a_0 = 1$, the spectral width of the scattered laser pulse must be about 50%. In addition, the exact nonlinear chirping in the expression for $\omega_{\mathrm{L,\,chirp}}$ is most likely not feasible in current and future experiments; at least no concrete ideas about the implementation of such chirping have been proposed. Thus, work on the precise nonlinear chirping of a scattered laser pulse to fully compensate the ponderomotive broadening remains a theoretical and numerical exercise, far from experimental implementation (although very useful for understanding the process and for further development).

The first experimentally realizable idea of compensating the ponderomotive broadening by using a linear chirp was proposed in 2019 in [167]. The idea was to roughly approximate the nonlinear chirp by a linear one using two pulses following each other, one of which approximates the increasing part of the frequency of the nonlinearly chirped pulse (i.e., has a positive linear chirp) and the second of which approximates the decreasing part of the frequency of the nonlinearly chirped pulse (i.e., has a negative linear chirp). It has been shown that such a two-pulse linear chirped scheme allows compensating the ponderomotive broadening to a good degree, achieving a narrow (from 2%) scattering line, and ensuring an increase in the number of scattered photons into a narrow line in approximate agreement with Eqn (11). Arguably, taking higher chirped orders into account in the two-pulse model would further improve the quality of the gamma source, especially the scattering line width.

An original method for the qualitative description of nonlinear Compton scattering based on considering the locus of stationary phase points of the scattering matrix integrals for different scattering angles was proposed in [168]. Using the methods of catastrophe theory, the presence of higher-order caustics in the spectrum of photons scattered at small angles was shown theoretically in the case of a linearly chirped laser pulse (an expression for the magnitude of a linear chirp as a function of a_0 is given in [168]); these caustics correspond to a narrow bright emission line with a width of the order of 2 to 3%.

We note that the overwhelming majority of studies on nonlinear Compton scattering are either theoretical or computational; in our opinion, very few experiments have been carried out. This is especially true of the problem of constructing narrow-band gamma sources for nuclear photonics. The last two of the schemes described above are relatively simple in implementation: producing linearly chirped laser pulses is a routine procedure. Experiments of this kind, first to test the concept and then to fully create high-luminosity gamma-ray sources, could be carried out in Russia by combining an electron accelerator with a laser system capable of generating laser pulses with a_0 of the order of unity with a spectral width of $\sim$ 5–20%.

3.5 Prospects for the development of Compton gamma sources

The development of laser systems has already led to a significant increase in the luminosity of Compton gamma sources. We list the main, in our opinion, new directions in the development of Compton sources of gamma radiation. First is a reduction in the size of sources due to the use of compact laser-plasma accelerators, including the replacement of all principal accelerating units (for example, focusing lenses) with laser-plasma ones [123]. This will make the construction of sources available to many laboratories and universities, and will significantly extend the geography of the use of gamma radiation in scientific research and in industry. Among other things, the availability of compact X-ray and gamma-ray sources based on laser-plasma accelerators in several universities will allow training highly qualified personnel for nuclear photonics. Second, a very promising direction is the use of nonlinear Compton scattering to create high-luminosity gamma sources (with the use of both standard and laser-plasma accelerators).

The new theoretical ideas presented recently regarding the use of high-intensity chirped laser pulses to create narrow-band bright gamma-ray sources are of interest to experimental groups, and it is likely that proof-of-concept experiments will be performed soon. We once again note the obvious advantage of using nonlinear Compton scattering over linear scattering: the increase in the number of photons scattered into a narrow line is proportional to a_0^2 (see Eqn (11)). Therefore, for example, the use of laser pulses with $a_0 = 1$ as opposed to $a_0 = 0.01$ increases the number of photons by four orders of magnitude. According to a rough estimate, we can expect that using (chirped) laser pulses with amplitude a_0 of the order of unity can increase the luminosity of modern sources by 2 to 4 orders of magnitude; for example, for an installation similar to ELI-NP, up to $10^{11}-10^{13}$ gamma photons per second can be expected in a line 0.5% in width.

4. General laws of photoabsorption of nuclei depending on the photon energy and new results for near-threshold energies

Turning to a description of the research program in nuclear photonics, we note that many classic photonuclear problems, including sum rules and radiation force functions, are now being solved at a new, improved level. The main research fields, depending on the energy of photons, are summarized in Table 1.

4.1 Optical anisotropy of nuclei

The most general definition of the processes under study (optical anisotropy of atomic nuclei) was given by Baldin [169]. It states that the cross sections of photonuclear

Table 1. Main research fields depending on the photon energy.

E_γ, MeV	Research field
Below 5	Astrophysics
5–10	Collective excitations of nuclei. Giant resonances. Pygmy resonances
30–150	Cluster states. Quasideuterons
150–2000	Nucleon resonances. Photoproduction of mesons. Statistical, dynamical, and spin structure of nucleons
Up to 10^6	Vector dominance, hadronization of photons

reactions are determined not only by the photon wavelength but also by the characteristics of the nuclei that interact with the electromagnetic wave. As a result, it becomes possible to measure various nuclear parameters, including mass, charge, and the anomalous magnetic moment, to study the spin characteristics of the nucleus, to determine the multipolarity of the interaction, and so on. Such studies were initially carried out for nuclei and subsequently were extended to nucleons.

According to de Broglie's formula, photon energy E is rigidly related to its wavelength λ:

$$\lambda = \frac{h}{p} = \frac{2\pi\hbar c}{E} \approx \frac{1234}{E} \text{ Fm} \tag{12}$$

(where energy is expressed in MeV).

In the framework of the plane-wave Born approximation (PWBA), the photon is regarded as an unbounded plain wave

$$\mathbf{A}(\mathbf{r}, t) = A_0 \mathbf{e}_\mathrm{p} \exp\left[\mathrm{i}(\mathbf{kr} - \omega t)\right] . \tag{13}$$

In recent years, there has been interest in studying the effects associated with the orbital angular momentum of a photon. It has been known to exist for about 100 years, but this problem was not addressed in earnest until the end of the 20th century, when the term 'twisted photons' appeared. But if a photon has an orbital angular momentum, then its front is distorted and turns into helical surfaces [170]. This is unrelated to the polarization of the photon, because polarization is associated with spin, not orbital angular momentum. An example of wave fronts of an electromagnetic wave with an orbital angular momentum is shown in Fig. 6.

If a photon is emitted in the course of a transition from a higher-spin nuclear state to a lower-lying state with a lower spin, the angular momentum of the nucleus changes. But because of the conservation law, the angular momentum can only be carried away by the emitted photon. Such a photon, according to modern terminology [170], is called twisted. The greater the multipolarity of the interaction, the higher the angular momentum of the photon as an individual particle, and it is quantized based on the multipolarity. As the multipolarity increases, the radiation probability decreases. Direct excitation of a higher-spin isomeric state of the nucleus, which would require the photon to have a sufficiently large orbital angular momentum, is therefore unlikely. This means that the isomer is being populated via a cascade, and the energy of the incident photon must be much higher than that of the isomer state, which is indeed observed in experiment. It is of interest to measure the energies of cascade

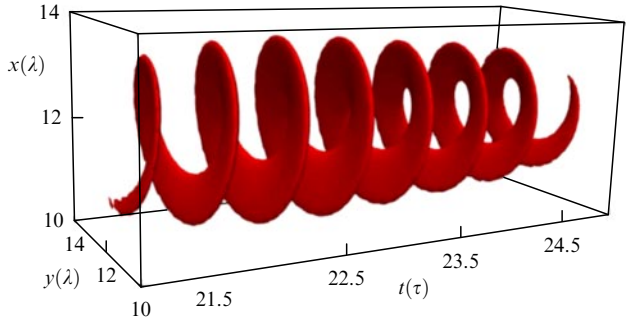

Figure 6. Example of wave fronts of a 'twisted' wave carrying an orbital angular momentum (from [171]).

gamma quanta and to determine their orbital angular momentum.

Twisted photons with a fixed value of the orbital angular momentum were first observed experimentally in the optical spectral range in 1992. In the nuclear energy range, twisted photons have not yet been detected, but they can be obtained using the (nonlinear) Compton backscattering method. This is because the main characteristics of photons (energy, momentum, and total angular momentum) are conserved in the process of Compton backscattering. This is confirmed by experiments on beams of polarized photons with energies up to several GeV [108], opening up new possibilities for studying the structure of nuclei.

4.2 Sum rules

To describe the nuclear photoabsorption cross section, the amplitude of the Compton scattering of a photon by a nucleon is introduced as [172]

$$f = \boldsymbol{\varepsilon}'^{*}\boldsymbol{\varepsilon} f_1(\omega) + \mathrm{i}\omega\boldsymbol{\sigma}\boldsymbol{\varepsilon}'^{*} \times \boldsymbol{\varepsilon} f_2(\omega) , \tag{14}$$

where $\boldsymbol{\varepsilon}$ and $\boldsymbol{\varepsilon}'$ are gauge-invariant operators of the electromagnetic field of the incident and scattered photons, $\boldsymbol{\sigma}$ is the spin operator of the nucleon, and ω is the energy of the photon. At $\omega = 0$ (the low-energy theorem),

$$f_1(0) = -\frac{\alpha M}{Z^2} , \quad f_2(0) = \frac{\alpha k^2}{2M^2} , \tag{15}$$

where M is the mass, eZ is the electric charge, and k is the anomalous magnetic moment of the nucleon. Dispersion relations allow connecting the scattering amplitude to the total photoabsorption cross sections of circularly polarized photons:

$$f_1(0) = -\frac{\alpha M}{Z^2} + \frac{\omega^2}{2\pi^2} \frac{\sigma_\mathrm{tot}(\omega')}{\phi(\omega')} \mathrm{d}\omega' , \tag{16}$$

$$f_2(0) = \frac{\alpha k^2}{2M^2} + \frac{\omega^2}{2\pi^2} \frac{\Delta\sigma_\mathrm{tot}(\omega')}{\phi(\omega')} \frac{\mathrm{d}\omega'}{\omega'} , \tag{17}$$

$$\begin{aligned} \sigma_\mathrm{tot}(\omega) &= \sigma_{3/2}(\omega) + \sigma_{1/2}(\omega) , \\ \Delta\sigma_\mathrm{tot}(\omega) &= \sigma_{3/2}(\omega) - \sigma_{1/2}(\omega) . \end{aligned} \tag{18}$$

Here, $\sigma_{1/2}$ and $\sigma_{3/2}$ are the photoabsorption cross sections where the photon spin and the nucleon spin are subtracted or added, depending on their mutual orientation.

Hence follows the Gerasimov–Drell–Hearn sum rule [173, 174], which relates the photoabsorption cross sections to the

fundamental characteristics of the nucleon:

$$k^2 = -\frac{2m^2}{\pi e^2}\int_{m_\pi}^{\infty}\frac{\sigma_{1/2}(\omega)-\sigma_{3/2}(\omega)}{\omega}\,\mathrm{d}\omega\,. \quad (19)$$

Another sum rule, first derived by Baldin [169], amounts to a relation between the electric (α) and magnetic (β) polarizability and the total photoabsorption cross section:

$$\alpha+\beta = \frac{1}{2\pi^2}\int_{m_\pi}^{\infty}\frac{\sigma_{\mathrm{tot}}(\omega)}{\omega^2}\,\mathrm{d}\omega\,. \quad (20)$$

Spin polarizability γ was deduced by Gell-Mann as [175]

$$\gamma = \frac{1}{4\pi^2}\int_{m_\pi}^{\infty}\frac{\sigma_{1/2}(\omega)-\sigma_{3/2}(\omega)}{\omega^3}\,\mathrm{d}\omega\,. \quad (21)$$

Despite its long history, the study of the sum rules is currently still a part of research programs of leading science centers, because new methods, mainly associated with the creation of new-generation gamma sources, make it possible to significantly refine nuclear data.

4.3 Total photoabsorption cross sections of nuclei and radiative strength functions

Currently, the total photoabsorption cross sections of nuclei are being studied in a wide range of energies, from the nucleon binding energy to several thousand GeV. At energies below 150 MeV, the total cross section is dominated by giant dipole resonance (GDR), whose maximum lies at about 20 MeV. This phenomenon has a universal character for all nuclei and has been studied in experiments in detail (see, e.g., review [176]).

At an energy of 20 MeV, the incident photon wavelength is close to 60 Fm, which is about five times the size of a heavy nucleus. According to the vibrational model [177], the nucleus enters the field of a wave that effectively acts on charged nucleons (protons) and excites vibrations whose frequencies are determined by the photon energy and the deformation of the nucleus. For spherical nuclei, the GDR width is about 3 MeV. For deformed axially symmetric nuclei, the resonance splits into two, while its width increases by about a factor of two.

At low photon energies, near the threshold, this simple approach does not work. The model has to be made more sophisticated by introducing surface effects, neutron halos, isospins, etc. (see, e.g., [178]). The isovector GDR is interpreted as a collective vibrational state with surface oscillations of neutrons relative to the central region of the nucleus. This mode is now called the pygmy dipole resonance (PDR) in the literature. Isoscalar dipole resonance can also lead to an exotic (toroidal) deformation due to surface vibrations. An effective tool in explaining the nature of the PDR is the quasiparticle phonon model in the random phase approximation (RPA), where partially hole excitations of nuclei are considered (see, e.g., [179]). The residual interaction is taken into account in calculating the PDR width.

In modern theoretical calculations in the framework of this model [180, 181], radiative strength functions are calculated, which reflect the reduced probabilities of radiative transitions from the ground state to an excited state or the probabilities of transitions between excited states. For an electrical transition with a multipolarity λL, the radiative strength function can be represented as

$$B(E\lambda)\uparrow_{\mathrm{arb.\,units}} = \frac{2\lambda+1}{4\pi}\left(\frac{3}{3+\lambda}\right)^2(1,\,2A^{1/3})^{2\lambda}\,(\mathrm{Fm})^{2\lambda}\,. \quad (22)$$

In Fig. 7, we show an example of theoretical calculations for tin nuclei in comparison with experimental data [181, 182]. The pygmy resonance turns out to be fragmented into a large number of transitions, which are not observed at high energies of gamma quanta.

Experimental studies of pygmy resonance are much fewer than theoretical ones. The main results have so far been obtained in traditional accelerator installations. Among them, in terms of the quality and volume of results, the HIGS setup at Duke University (USA) stands out, where a beam of monochromatic polarized photons with an intensity of about 10^8 photons per second was obtained by the method of Compton backscattering [183].

In the experiment, the separation of transitions by multipolarity is effected by measuring the asymmetry in the angular distributions of scattered photons. For this, high-resolution detectors are placed at angles along and across the direction of the incident beam. The dominant contribution of the GDR for all nuclei of the periodic table was thus confirmed experimentally. In addition to this general conclusion, it is too early to speak about any individual peculiarities of pygmy resonance in different nuclei, because no classification has yet been worked out.

At photon energies above 20 MeV, up to the meson production threshold, a significant contribution is made by the so-called quasideuteron photoabsorption mechanism [184]. When the wavelength of gamma quanta becomes comparable to the size of the deuteron, the cross section is described by Levinger's phenomenological formula

$$\sigma_{\mathrm{tot}} = L\,\frac{NZ}{A}\,\sigma_{\gamma\mathrm{d}}(E_\gamma)\exp\left(-\frac{E_\gamma}{S_\lambda}\right), \quad (23)$$

where $\sigma_{\gamma\mathrm{d}}(E_\gamma)$ is the photodisintegration cross section of a free deuteron, and $L\approx 10$ and $S = 60$ MeV are fitting parameters.

At incident photon energies above ≈ 150 MeV up to 2 GeV, a region can be identified where the photoproduction of mesons on quasifree nucleons of the nucleus dominates. Therefore, the total photoabsorption cross sections, when normalized to the number of nucleons in the nucleus, are practically the same for nuclei heavier than beryllium. This dependence is called the universal curve [185]. However, in Novosibirsk, deviations from the universal dependence were found in a beam of Compton photons for heavy nuclei [186]. These results were later confirmed in experiments with a beam of tagged bremsstrahlung photons at the Jefferson Laboratory (USA) [187]. On the whole, this indicates the existence of new photoabsorption mechanisms in the region of nucleon resonances, which have not yet been given a theoretical explanation.

At photon energies above 2 GeV and up to 200 GeV, the $\sigma_{\mathrm{tot}}/A\sigma_{\gamma\mathrm{p}}$ ratio becomes less than unity (for lead, by about 20%) in the entire region considered. This effect is explained by the vector dominance model [188], according to which a photon at an energy above the vector meson production threshold (which is 1090 MeV for the ρ meson) starts behaving like a strongly interacting particle. At high energies, in other words, part of the time, the photon behaves like a photon, and part of the time, like a hadron that interacts

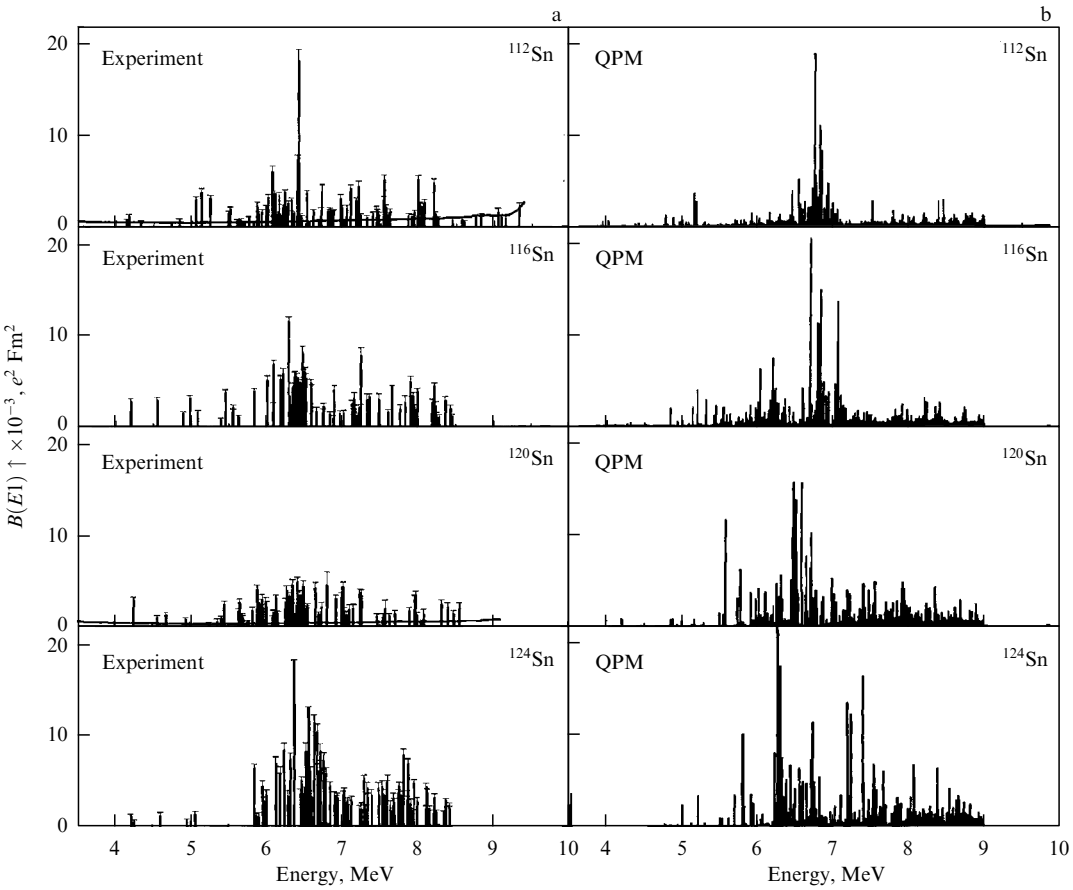

Figure 7. Radiation strength functions for tin nuclei [181]. (a) Result of experiments using the S-DALINAC accelerator in Darmstadt. (b) Result of theoretical calculations in the framework of the quasiparticle model taking three-phonon states into account.

only with surface nucleons. Theoretical calculations of the total photoabsorption cross sections at high energies in the framework of the vector dominance model give a stronger dependence on the atomic number than was found experimentally. More detailed information on the general laws of photoabsorption of nuclei in a wide range of photon energies can be found in [189].

4.4 Virtual photons

The close relation between the action produced by a charged particle and electromagnetic waves was first noted by Fermi [190]. Weizsäcker [191] and Williams [192] then showed that the effect of the passage of an electron near a nucleus can be described using the virtual photon spectrum $N_e(E_e, E_\gamma)$ that is close in shape to the bremsstrahlung spectrum. The equation for these spectra is given in a convenient form in [193]:

$$N_e^{\lambda L}(E_e, E_\gamma) = \frac{\alpha}{\pi}\left(\left[1+\left(\frac{E_e - E_\gamma}{E_e}\right)^2\right] \times \ln\frac{2E_e(E_e - m_e)}{m_e E_e} - C_L\right), \qquad (24)$$

where α is the fine structure constant, λL is the multipolarity of the interaction, $C_L = 2(E_e - E_\gamma)/E_e$ for $\lambda L = E1$ (electric dipole transition), $C_L = 0$ for $\lambda L = M1$ (magnetic dipole transition), and $C_L = 8/3(E_e - E_\gamma)^2/E_e^2$ for $\lambda L = E2$ (electric quadrupole transition). Here, L is a number expressing multipolarity.

The calculated spectrum of virtual photons in the PWBA and the distorted wave Born approximation (DWBA) for the electron energy of 10 MeV is shown in Fig. 8. It can be seen that, at low energies of virtual photons, the multipolarity of the interaction, in contrast to real photons, increases significantly. This opens up the possibility of studying the nature of collective vibrations of nuclei with an exotic shape and deformation, not merely dipole excitations. However, the first experimental data indicating a change in the multipolarity of the near-threshold absorption of virtual photons were obtained only relatively recently [7]. The measurements were carried out with the linear electron accelerator LUE-8-5 using the method of induced nuclear activity for the reactions $^{111}\mathrm{Cd}(\gamma,\gamma')^{111m}\mathrm{Cd}$, $^{113}\mathrm{In}(\gamma,\gamma')^{113m}\mathrm{In}$, $^{115}\mathrm{In}(\gamma,\gamma')^{115m}\mathrm{In}$. Because the energy of isomeric states for these nuclei does not exceed 300 keV, the isomeric ratios are weakly dependent on the energy of photons with energies above 5 MeV. Comparing the yields of reactions induced by virtual and real photons allowed drawing conclusions about the dependence of the total photoabsorption cross sections on the multipolarity. The measurement result is shown in Fig. 9.

We now clarify what is meant by the yield per equivalent photon $\sigma_q(E_e, E_\gamma)$ and by the inclusive yield per electron $\sigma_e(E_e, E_\gamma)$, whose ratio is shown in Fig. 9. Because the spectra of real (bremsstrahlung) and virtual photons, $N^{\lambda l}_{\gamma,\mathrm{real}}$ and $N^{\lambda l}_{\gamma,\mathrm{virt}}$, are continuous, the integral over the entire spectrum is measured in experiment:

$$\sigma_q(E_e) = \frac{E_e\int_0^{E_e} N^{\lambda l}_{\gamma,\mathrm{virt}}(E_e, E_\gamma)\sigma_\gamma(E_\gamma)\,\mathrm{d}E_\gamma/E_\gamma}{\int_0^{E_e} N^{\lambda l}_{\gamma,\mathrm{virt}}(E_e, E_\gamma)\,\mathrm{d}E_\gamma}, \qquad (25)$$

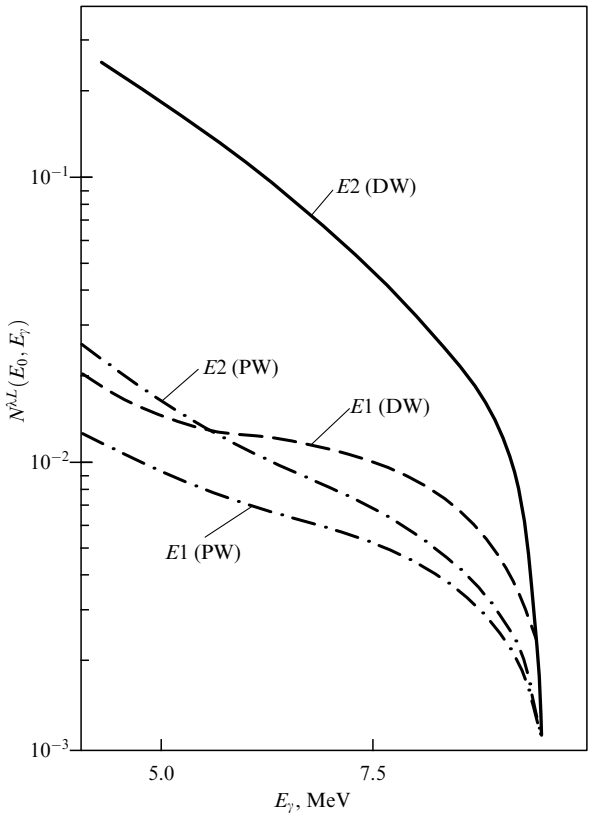

Figure 8. Spectrum of virtual photons in the PWBA for a heavy kernel ($Z = 92$) at the electron energy of 10 MeV [194].

$$\sigma_e(E_e) = \frac{E_e \int_0^{E_e} N^{\lambda l}_{\gamma,\,\mathrm{real}}(E_e, E_\gamma)\sigma_\gamma(E_\gamma)\,\mathrm{d}E_\gamma/E_\gamma}{\int_0^{E_e} N^{\lambda l}_{\gamma,\,\mathrm{real}}(E_e, E_\gamma)\,\mathrm{d}E_\gamma}\,. \qquad (26)$$

We can see from Fig. 9 that the experimental results are fundamentally different from the model predictions made both in the PWBA and in the DWBA. This indicates a change in the multipolarity of photoabsorption near the threshold. Possibly, this is due to collective excitations of exotic nuclei (toroidal, scissor, and compression vibration modes) predicted in the framework of the existing models. This is an indirect statement, based only on theoretical assumptions. However, there are quite a few similar examples in nuclear physics. We note the study of shape isomers, or spontaneously fissioning isomers, in actinide nuclei [195]. This phenomenon has been explained in the model of a two-humped fission barrier, although direct measurements of the moments of inertia and deformation parameters of isomeric nuclei have not yet been made. Various experimental methods, including the identification of the rotational band in the gamma spectrum of excited nuclei or optical methods for measuring the isomeric shift are discussed in [196], but none of them has been developed further. The question of the experimental determination of the spectra of virtual photons was also discussed earlier [189], but no continuation followed.

We note that nuclear excitations by virtual photons are now being actively studied in reactions with relativistic atomic nuclei. In this case, methods are used that were developed previously in electronuclear experiments. For example, the method of virtual photons is used in studying the Coulomb dissociation of nuclei. However, the terminology and model description of collective excitations, including GDR, are very different from photonuclear interpretations of this phenomenon. Unfortunately, a detailed discussion of this subject is beyond the scope of this review, but we hope that the review will help unify different approaches to the problem under study.

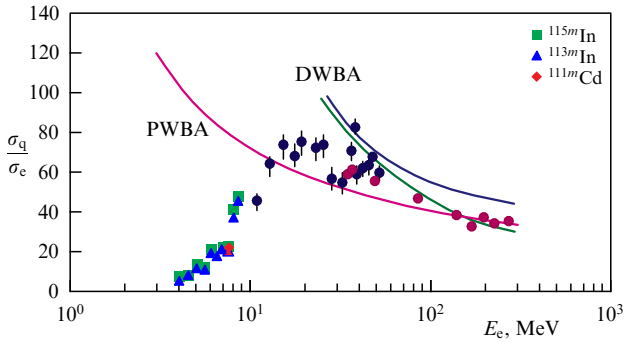

Figure 9. Ratio of the photoexcitation cross sections by real and virtual photons with an energy up to 10 MeV for ^{111m}Cd, ^{113m}In, ^{115m}In nuclei. Triangles: data in [7], dots: data from the literature, as quoted in review [189]. Lines: result of PWBA and DWBA computations.

4.5 Photonuclear processes with high-power lasers

A number of interesting results have been obtained with gamma-ray beams arising under the action of superstrong laser radiation on a dense target. In the historically first work [197], the activation of a copper target due to ^{63}Cu(γ, n)^{62}Cu and ^{65}Cu(γ, n)^{64}Cu reactions was investigated; the activation was used to estimate the flux of gamma quanta with energies above 10 MeV that formed under irradiation by the VULCAN laser of the Rutherford Laboratory (25 J, 1 ps, 10^{19} W cm^{-2}). Papers [198, 199], which appeared shortly after, reported a wide range of photonuclear reactions on ^{11}C, ^{38}K, ^{62,64}Cu, ^{63}Zn, ^{106}Ag, ^{140}Pr, ^{180}Ta, and ^{197}Au nuclei, as well as nuclear photofission of ^{238}U with a VULCAN laser and a superpower 0.5-PW laser from the Livermore Laboratory. The nuclear activation technique was used in [200] to estimate the quasitemperature of the gamma beam. A number of photonuclear reactions were realized in [201], including the ^{9}Be(γ, n)2α reaction with a low (1.5 MeV) threshold. In [202], a femtosecond laser with a high (10 Hz) repetition rate of short (50 fs) pulses (intensity $(3-5)\times 10^{19}$ W cm^{-2}) was used for the first time. It was possible to estimate the cross sections for a number of (γ, p)-type reactions for ^{25}Mn, ^{48,49}Ti, ^{68}Zn, and ^{97,98}Mo targets. We note the measurement of the deuteron photodisintegration cross section in the (γ, n) reaction at the threshold [203] (Fig. 10), carried out with a terawatt laser. On the whole, however, there have been practically no fundamentally new nuclear physics results so far.

It is of interest to compare the parameters of electron beams with energies up to 10 MeV obtained in conventional and laser–plasma electron accelerators [113, 205]. As an example, in Table 2 we show data for the LUE-8–5-MeV linear electron accelerator at the INR and the terawatt femtosecond laser complex at Lomonosov Moscow State University (wavelength 800 nm, pulse duration 50 fs, repetition rate 10 Hz, pulse energy up to 50 mJ, peak intensity on the target up to 10^{19} W cm^{-2}). The electron acceleration mechanisms with such strong laser radiation in the case of a solid-state target have been discussed above.

Gamma beams can be produced by transforming an electron beam in a thick metal plate.

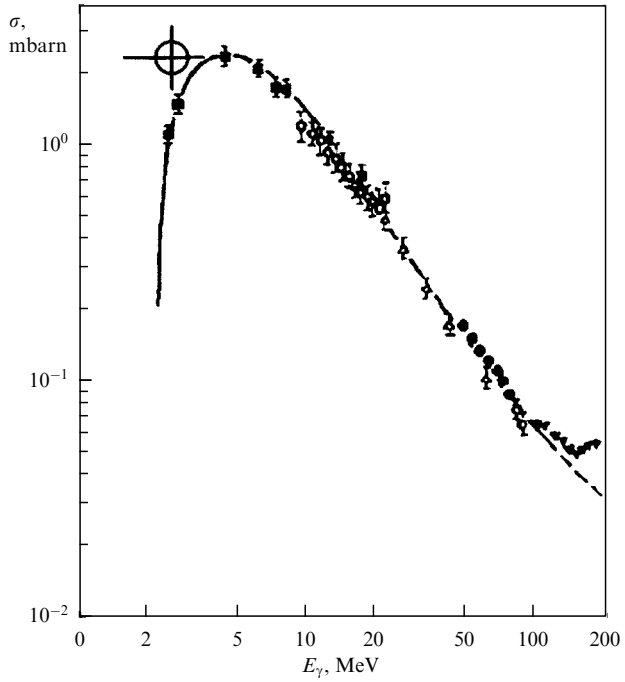

Figure 10. Cross section of the D(γ, n)H reaction [204]. Stand-alone dot shows the value obtained at a laser facility with $E_\gamma = 3.6 \pm 0.3$ MeV [189].

Table 2. Parameters of electron beams attained with LUE-8-5 and with the the MSU femtosecond terawatt laser.

	LUE-8-5	MSU laser–plasma accelerator
Electron spectrum, MeV	Monochromatic, tunable in the range 5–9, spectrum width 1%	Exponential with a 'slope' 2–5
Pulse repetition rate, Hz	100	10
Pulse duration, μs	3	10^{-7}
Average beam current, μA	3 – 10	3×10^{-4} (above 1 MeV)
Total beam current, A	5×10^{-2}	30
Emitter focus, mm	4	4×10^{-3}
Angular divergence, mrad	0.1	2

In Fig. 11, we show the energy and angular distributions of photons emitted from a stopping tungsten target 0.4 mm thick, which, according to simulations, is optimal from the standpoint of the obtained photon yield. Because the laser and accelerator beam intensities differ greatly, the exposure time was taken as a parameter for comparing the yields, for the photon yield to be estimated on an absolute scale.

We see that studying photonuclear reactions currently requires beams of hard gamma quanta in a wide range of energies. Such beams can be obtained with both traditional electron accelerators and laser–plasma accelerators. In the first case, beams can be continuous for studying the products of photonuclear reactions in coincidence mode; laser beams, on the other hand, can provide unique time parameters for

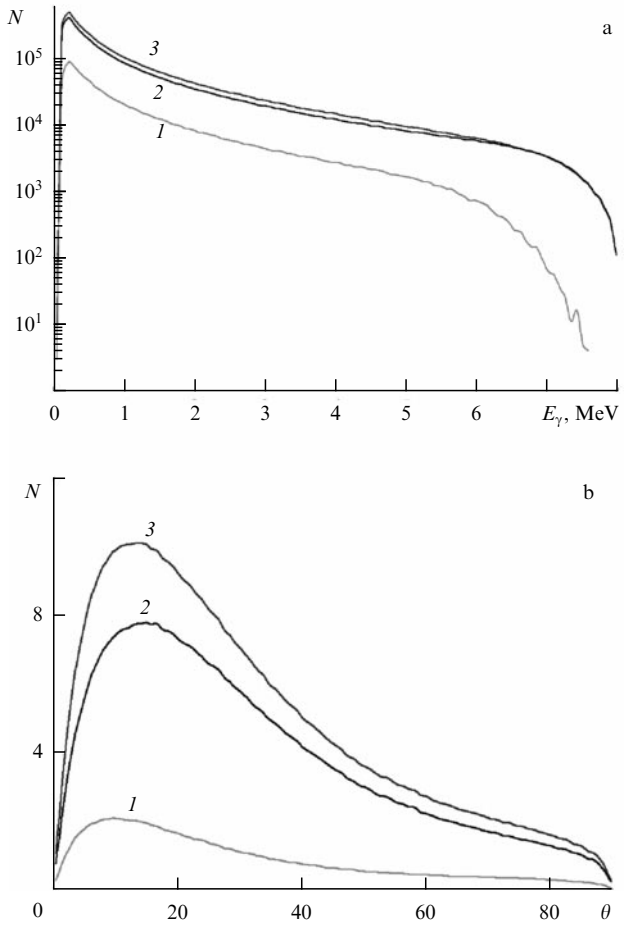

Figure 11. (a) Energy and (b) angular distribution of bremsstrahlung photons (in rel. units). Lines *1* and *2* correspond to single and double scattering; line *3* shows the full spectrum [206].

pulsed neutron sources, positron spectroscopy, and X-ray and gamma tomography.

4.6 Low-energy isomeric states

A promising area of research for nuclear photonics is the study of states of nuclei with low energies on nuclear energy scales [94, 207]. They can be both isomeric states with energies less than 50 keV relative to the ground state of the nucleus and metastable states with energies of about 1 MeV and above, near which (with an energy difference up to 50 keV) states with much shorter lifetimes can be located. Without a doubt, the study of isomeric states of nuclei is of fundamental interest. In addition, the accumulation of energy in an ensemble of metastable isomers with their subsequent discharge via a closely lying level can be used to create nuclear energy sources [208, 209] and to obtain population inversion under nuclear transitions [207, 210–214]. Long-lived isomeric states (and radiative transitions from such states) can serve as frequency standards [215–218] in implementing quantum computations [219] and in other applications.

Such isomers are primarily studied with synchrotron sources [220, 221]. Betatron or Thomson X-ray sources may be alternative sources for the excitation of nuclear isomers with energies of 1 keV or more. For a betatron source [115], the characteristic flux of quanta with energies of 1 to 10 keV can reach 10^5 photons s^{-1} eV^{-1} $mrad^{-2}$ for a

laser pulse repetition rate of 1 to 10 kHz. For a Thomson generator based on a linear accelerator with an electron energy of 20–30 MeV and a picosecond laser, the number of quanta can reach 10^8 photons s^{-1} eV^{-1} $mrad^{-2}$. For a Thomson generator based on a linear accelerator with a storage ring and a laser storage cavity, the number of quanta can reach 10^9 photons s^{-1} eV^{-1} $mrad^{-2}$ and over more, but for optimization for the spectral range of 1–10 keV, the energy of accelerated electrons must be low (20 MeV), which is not typical for modern designs of such generators. Much higher fluxes are provided by free electron lasers (XFELs) [222], whose luminosity can exceed the luminosity of SR sources by eight or more orders of magnitude [223].

An important advantage of using laser sources over approaches that are traditional for nuclear physics experiments is the possibility of simultaneous or time-synchronized production of metastable states and their excitation using one laser system in the framework of a single experiment. The X-ray and electron laser sources are used here to excite isomeric states while gamma, proton, and neutron laser sources are used to create metastable states or unstable isotopes with a suitable structure of closely lying levels.

Experimental data on the energies and/or lifetimes of a number of low-energy isomers, even for stable or long-lived isotopes, have appeared only recently or are still lacking. For example, the lifetime of the ^{201m}Hg isomer with an energy of about 1.5 keV was first experimentally estimated in 2004 [224]. The existence of an isomeric state for the ^{229}Th isotope has long been assumed from indirect measurements [225, 226], but only in the last few years has the energy of this state been substantially refined, from 3.5 to 8 eV [227, 228], and the lifetime of this isomer measured, amounting to about 7 μs [229], with the radiation lifetime remaining unknown (estimated at 3 h).

The excitation of isomeric levels directly in a dense laser plasma is also being actively investigated. In the plasma environment, the spectrum of possible mechanisms for the excitation of low-lying isomers of nuclei expands significantly [230, 231] (Fig. 12): in addition to photoexcitation by the proper X-ray radiation of the plasma and inelastic scattering of plasma electrons, there are mechanisms associated with the excitation of a nucleus by a virtual photon via the atomic shell, NEET and NEEC (the excitation by a photon emitted in a bound–bound transition of an electron in the atomic shell or in the recombination of a free electron, respectively), and other higher-order processes. We note that, for these two processes, at least one of the electron states is bound, which is not shown in the diagram in Fig. 12b. In addition, the decay channels of isomeric states via the atomic shell are also significantly modified due to its ionization and the corresponding shift of ionization potentials [232], as well as due to a shift in the potential induced by the plasma environment [233]. Experimental and theoretical approaches to the excitation of nuclear levels in laser plasmas are discussed in detail in the 2001 review [207], which notably covers the use of the hot dense plasma produced by high-power femtosecond laser pulses [234]. Since then, a number of experimental studies have been performed [235–237], but reliable observation of the effect remains an open question.

Recently, a number of theoretical and computational studies have been devoted to the analysis of NEET [238] and NEEC [223, 239–242] processes in hot plasma in the case of excitation from metastable levels of ^{93m}Mo isomers (state energy of 2.4 MeV; transition occurs to a short-lived level

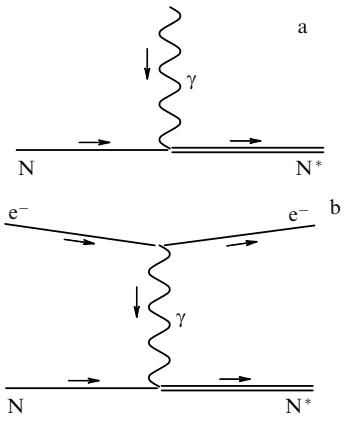

Figure 12. Transition of a nucleus from ground state N to excited state N* in plasma (a) under photoexcitation and (b) in the processes of inelastic scattering of an electron on the nucleus (free–free electron transition), NEET (bound–bound electron transition), and NEEC (free–bound electron transition).

separated by 4.85 keV and related to the ground state of the nucleus by radiative transitions) and ^{84m}Rb (463 and 3.5 keV, respectively). For example, it was shown in [223, 239] that the plasma formed by an XFEL radiation beam [243] significantly changes the probability of the excitation of the ^{93m}Mo isomer by the NEEC mechanism, increasing this probability by six orders of magnitude, and it is this excitation channel (not direct photoexcitation) that becomes dominant. In [241, 242], the probability of NEEC of the same isomer in a plasma produced by high-power femtosecond laser systems was calculated, and a further increase in this probability by another six orders of magnitude was revealed, which allows obtaining an experimentally detectable effect of isomer 'discharge' at a laser pulse energy of 100 J or more. It is also noted there that additional ionization of deep atomic shells by XFEL radiation simultaneously with the creation of plasma by a powerful laser pulse can lead to a further increase in the probability of the NEEC process. On the other hand, the experimental observation of hollow ions and the associated estimates [244, 245] show that the power density of X-ray radiation proper inside such a plasma can reach 5×10^{18} W cm^{-2} or more (at the on-target laser power density of 10^{20} W cm^{-2}), which greatly exceeds the XFEL radiation power density (about 10^{17} W cm^{-2}). In particular, this means that the probability of the initiation of transitions between low-energy nuclear states in a hot dense plasma can be much higher than follows from earlier calculations.

At present, the ^{229m}Th isomer with a remarkably low energy of 8 eV and total lifetime of 7 μs is very actively being discussed and investigated (see review in [218, 246]). Various schemes for its laser excitation are being considered [247, 248]. Experimental studies of this isomer are currently being carried out by research groups in Germany (Ludwig-Maximillian University, Munich) and in Russia (Lebedev Physical Institute, Russian Academy of Sciences, Moscow). In particular, it was established experimentally that the energy of this level is 8.28 ± 0.17 eV [224]. The isomeric level was first populated in [249] using synchrotron radiation via a higher level with an energy of 29 keV.

Of fundamental importance for the problem under consideration is the implementation of direct excitation of the isomeric state ^{229m}Th using narrow-band laser radiation [223], which is usually taken to be a higher harmonic of

optical laser radiation that is in resonance with the isomeric nuclear transition [236], or radiation from a free electron laser [250]. Effective harmonic generation at a wavelength of about 150 nm is a rather difficult task; high-pressure gas jets are used as a nonlinear optical medium [251, 252].

At the same time, the effect of electromagnetic radiation from an external laser source on the atomic shell of the same nucleus in which the excitation of a low-lying isomeric state is studied can also lead to the excitation of this nucleus via a process that is essentially very close to the traditional process of generation of higher optical harmonics. Indeed, a three-stage model is used to semiquantitatively describe the higher harmonic generation by an atom [253]: first, a linearly polarized optical field causes tunneling ionization of the atom; next, a free electron returns to the original atom under the action of the optical field; and, finally, the electron recombines and a photon is emitted. The maximum photon energy of recombination radiation is determined by the sum of the ionization energy of the atom and the maximum energy of the electron in an external field, $E_e \approx 3.17(eE\lambda)^2/(16\pi^2 mc^2)$. The discrete spectrum of odd harmonics is formed due to the periodicity of the process of interaction with the optical field.

Let us discuss this process from the standpoint of the excitation of nuclei. An electron returning to its original atom belongs to the continuous spectrum of states. Excitation of a nucleus can occur, by analogy with processes in plasma, due to (1) emission of a recombination photon that is in resonance with a nuclear transition, i.e., a process similar to NEEC; (2) inelastic scattering of an electron by a nucleus, i.e., a process similar to nuclear excitation electron scattering [254]; (3) recombination of an electron to an excited atomic level with the subsequent emission of a photon in resonance with the nuclear transition, i.e., a process similar to NEET, etc. We note that process (3) is observed during the generation of higher harmonics, leads to the resonant amplification of a certain harmonic [255], and is explained by the electron capture by a Rydberg state of the atom [256].

The fundamental difference between the processes under consideration and processes in plasma consists in a much higher cross section, because the impact parameter in the scattering of an electron by a nucleus is rather small and the recombination radiation must be considered in the near field of the atom (or the nucleus). In [257], the effect on a thorium atom of two-frequency radiation of a titanium-sapphire laser (first and second harmonics at wavelengths of 750 and 375 nm) was considered for the first time, and the fifth harmonic field was calculated. In that case, in addition to the generation of even optical harmonics, it becomes possible to control the angular momentum of the total optical field, which can lead to a significant increase in the efficiency of excitation of high-multipolarity nuclear transitions.

Figure 13 shows the dependence of the maximum cutoff energy E_e on the optical field strength; the energies of isomeric states of a number of isotopes are also indicated. It can be seen that the ^{229m}Th and ^{235m}U isomers can be excited at optical field strengths typical of the regime of generation of higher harmonics; for a number of other isomers, this requires fields of the order of the atomic field. Approaching the 'boundary' of the relativistic interaction regime means that the electron packet is deflected from the parent atom by the magnetic component of the field, and the collision (recombination) cross section decreases. This is a well-known effect in the generation of higher harmonics, and several approaches have been proposed to partially suppress it by controlling the field polarization, using several optical beams, and so on [256].

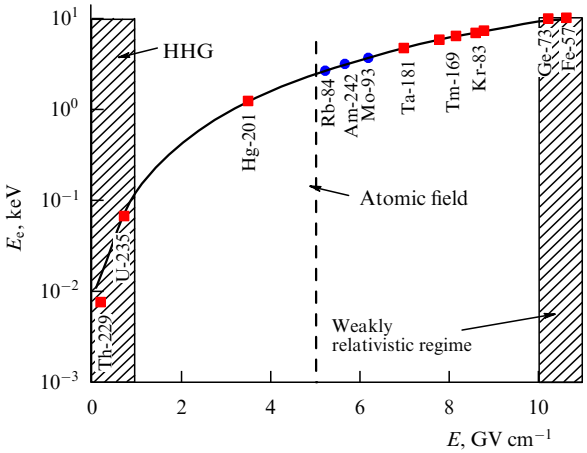

Figure 13. Dependence of the maximum energy E_e of higher harmonics on the optical field strength (wavelength 800 nm). Symbols show the energies of low-lying isomeric states of a number of stable isotopes (squares) and the energy transition to the nearest level from metastable states (circles). Shaded area on the left corresponds to the range of field strengths typical of higher harmonic generation (HHG), and that on the right, to the weakly relativistic interaction regime. Vertical dashed line shows atomic field strength.

5. Interdisciplinary and applied research

5.1 Astrophysics

The study of photonuclear reactions has rather diverse and numerous astrophysical applications. Among them are the following:

• Precision and model-independent measurements of neutron distribution in heavy nuclei (the radius and the outer layer at average density $\rho = 0.1$ Fm^{-3}) would allow constructing an equation of state for neutron stars at a higher density and determining the liquid-to-solid phase transition point. In this regard, we note the encouraging results of classical experiments on electron scattering, including the measurement of the weak form factor involving parity violation, because neutrons have no electric charge [258].

• Investigation of Coulomb interaction reactions to estimate the radiative capture cross sections at energies below the nucleon binding energy for short-lived radioactive nuclei has allowed describing the mechanisms of the explosion of novae, supernovae, and neutron stars [259].

• Investigation of photoneutron reactions on light nuclei (D, Be) at photon energies from 1 to 3 MeV allowed obtaining data on backward reactions that are essential for the early stage of the formation of the Universe [260].

• Measurement of the bremsstrahlung spectrum of cosmic rays allowed estimating the Planck thermal spectrum for the γ process at temperatures up to 2.5 MeV. The study of fluorescence under irradiation of ^{196}Au provided information on the electron capture processes in nuclei [261].

• The study of unstable nuclei with colliding electron and relativistic ion beams by the classical method of electron scattering provides information on inelastic interactions of neutrinos with nuclei, which allows studying various nucleosynthesis mechanisms (r-process, explosive and delayed

processes) and thermalization processes during the collapse of stars [262].

Directly related to nuclear photonics is the absolute measurement of the position of the upper bound of the Compton gamma-ray spectrum in order to measure the anisotropy of the speed of light relative to the cosmic microwave background (CMB) dipole [263]. We discuss this result in somewhat greater detail.

The dipole anisotropy of the CMB at temperature T has a Doppler nature:

$$\frac{\delta T(\theta)}{T} = \frac{v}{c}\cos\theta + \frac{v^2}{2c^2}\cos 2\theta + O\left(\frac{v^3}{c^3}\right). \qquad (27)$$

The first term denotes the dipole term, which is determined by the speed of Earth's motion: $v/c = 0.000122 \pm 0.00006$, $v = 365 \pm 18$ km s^{-1} in the reference frame associated with the CMB.

Earlier satellite experiments and Mössbauer laser spectroscopy experiments [264] yielded the upper bound for the anisotropy value $\delta c/c$ at the level of 2×10^{-10}. The work done in [263] is analogous to the classic Michelson–Morley experiment, but the result was obtained in a completely independent way, which allowed improving the accuracy by two orders of magnitude. To determine the anisotropy of the speed of light with respect to the CMB dipole, a beam of gamma quanta obtained by Compton backscattering of electrons in a storage ring was used. The experiment was carried out by the GRAAL collaboration at the European Synchrotron Radiation Facility (ESRF) in Grenoble [265].

The method is based on measuring the position of the upper edge of the Compton radiation spectrum depending on the orientation of the facility (Earth) in space. The Lorentz factor for the electron $\gamma = 1/(1-\beta^2)^{1/2}$ satisfies the equation

$$\beta\,\mathrm{d}\beta = \frac{1}{\gamma^2}\frac{\mathrm{d}\gamma}{\gamma}, \qquad (28)$$

whence anisotropy acquires the factor $1/\gamma^2 \approx 10^8$, which allows increasing the measurement accuracy by eight orders of magnitude. At the GRAAL facility, the electron energy in the storage ring was 6027.6 ± 0.6 MeV and the laser radiation wavelength was 514 or 351 nm. The position of the upper edge of the Compton photon spectrum was measured using a microstrip tagging system with a step of about 6 MeV, and no worse than 10^{-4} for the center of gravity.

As a result of these measurements, the value $\delta c/c = 3 \times 10^{-12}$ was obtained, which is two orders of magnitude more accurate than the results available previously. More information on this subject can be found in [266, 267].

A new impetus to the development of work on laboratory nuclear astrophysics can be imparted by the use of laser–plasma accelerators and hot plasma as a source of accelerated particles, because the plasma state typical for most astrophysical problems and the energies and fluxes of laser-accelerated particles will in the near future be comparable to or — by some parameters — even exceed the energies and fluxes of traditional accelerator complexes [268]. In [269], a number of problems were identified whose solution can be effectively aided by high-power fetmosecond lasers (see also [270]): the lithium problem of the low abundance of the ^{7}Li isotope; the search for reactions that provide a neutron flux for the so-called s-process, which determines the abundance of elements with a nuclear charge from $Z = 26$ (Al) to $Z = 82$ (Pb); refinement of the formation mechanisms of bypassed stable p-nuclei of the type ^{74}Se, ^{78}Kr, ^{84}Sr, ^{92}Mo, ^{96}Ru, ^{180}Ta, etc.; and the study of photonuclear reactions with isotopes and isomers used in astronomical observations (^{26}Al, ^{60}Fe, etc.).

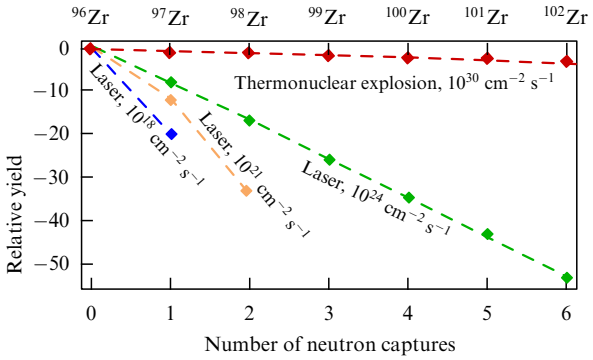

Figure 14. Relative yield (on a logarithmic scale) of isotopes as a result of sequential capture of neutrons (r-process). Original ^{96}Zr target [99].

Within the ELI-NP research program, significant attention will be paid to the study of both p-processes and photonuclear reactions (γ, n), (γ, p), (γ, α). At the same time, a number of experiments can be carried out on compact laser systems, where a significant advantage can come from the high average particle flux. For example, observations of the reaction $^{181}\mathrm{Ta}(\gamma, \mathrm{n})^{180}\mathrm{Ta}$ with the threshold 7.6 MeV and a number of reactions $^7\mathrm{Li}(\mathrm{p}, \mathrm{n})^7\mathrm{Be}$, $^{63}\mathrm{Cu}(\mathrm{p}, \mathrm{n})^{63}\mathrm{Zn}$, $^{48}\mathrm{Ti}(\mathrm{p}, \mathrm{n})^{48}\mathrm{V}$ with threshold energies from 1.88 to 5 MeV were reported in [201] with the use of a picosecond laser complex with a peak power of 10 TW.

An urgent task is to study the r-process, the sequential capture of several neutrons by the nucleus with the subsequent formation of a new heavy stable (or long-lived) nucleus, which is believed to be responsible for the nucleosynthesis of heavy stable isotopes with an atomic weight above 209 [271] and, partially, for isotopes heavier than Fe [272]. Taking the typical decay times into account, the r-process is considered possible for neutron fluxes above 10^{20} s^{-1} cm^{-2} [273], which greatly exceeds the neutron fluxes attainable with current neutron generators [99] and is comparable to the neutron flux produced by an exploding thermonuclear bomb [274].

An alternative source of laser-induced neutrons in the near future may be the implementation of the spallation process, when a target is irradiated with fast laser-accelerated protons; peak neutron fluxes can then reach 10^{24} s^{-1} cm^{-2}. For example, when using multipetawatt laser systems created within the ELI project, more than $> 10^{12}$ neutrons should be expected in a 0.7 ns pulse in a lead target, with a neutron flux of 10^{22}–10^{23} s^{-1} cm^{-2}. Further optimization is expected to increase these flows by one to two orders of magnitude. Figure 14 taken from [99] presents the results of calculations of the possible number of successive neutron captures for the ^{96}Zr isotope at various peak neutron fluxes. Neutron sources involving modern high-power lasers provide a neutron flux of 10^{18} s^{-1} cm^{-2} in a pulse about 1 ns in duration, which corresponds to the s-process (capture of only one neutron). When using commissioned multipetawatt laser systems, the expected flux will reach 10^{24} s^{-1} cm^{-2}, which already ensures the capture of several neutrons. For comparison, Fig. 14 also shows the calculated dependence for a single microsecond neutron pulse due to a thermonuclear explosion. Table 3

Table 3. Comparative characteristics of several neutron sources.

Facility	Peak neutron flux, n s^{-1} cm^{-2}	Average neutron flux, n s^{-1} cm^{-2}	Neutron pulse duration, ns	Repetition rate, Hz	Reference
ILL	$\sim 10^{15}$	$\sim 10^{15}$	Continuous	Continuous	[275]
SNS	$\sim 10^{16}$	$\sim 10^{12}$	1000	60	[275]
Operational laser sources	$\sim 10^{18}-10^{19}$	$\sim 5\times10^{5}-5\times10^{6}$	1	5×10^{-4}	[97, 276, 277]
Laser sources under construction	$\sim 10^{22}-5\times10^{24}$	$10^{11}-5\times10^{13}$	0.1 – 1	0.1 – 0.01	See Section 2.1
NIF (National Ignition Facility)	$> 10^{26}$	$> 10^{10}$	0.01	10^{-5}	[274]

presents comparative characteristics of various neutron sources.

5.2 Isotope transmutation

One of the most promising methods for the transmutation of long-lived nuclear isotopes is irradiation of a sample containing such isotopes with gamma radiation or neutrons, resulting in the formation of a new isotope with a much shorter lifetime [4, 278]. This is important for the decontamination of the spent fuel of modern nuclear power plants (which contains a number of long-lived isotopes in high concentrations, including ^{129}I and ^{135}Cs). In the absence of reprocessing, spent fuel must be stored for hundreds of thousands of years; modern methods of reprocessing and separating isotopes reduce the required storage time by an order of magnitude, and transmutation can reduce this time by another two orders of magnitude, to several hundred years, while reducing the volume of stored waste 100-fold. At present, it is believed that effective transmutation can be carried out by irradiating samples with neutrons generated during spallation using a proton beam from a linear accelerator (e.g., the European project MYRRHA [279]).

In [280], laser-induced transmutation of the ^{129}I isotope with a lifetime of 15.7 million years into the ^{128}I isotope with a lifetime ~ 25 min was first demonstrated experimentally in the reaction $^{129}\mathrm{I}(\gamma,\mathrm{n})^{128}\mathrm{I}$. Gamma radiation was obtained by irradiating a thick gold target with a laser pulse with the intensity of 5×10^{20} W cm^{-2}. The cross section of this process was also estimated as 97 ± 40 mbarn. A number of recent studies are devoted to the analytic and computational substantiation of the choice of optimal schemes for generating a gamma beam for transmutation and the laser radiation parameters used for this [281–284]. In general, we can conclude that the approaches based on laser-induced generation of gamma radiation are currently inferior to more traditional approaches based on electron accelerators, but the development of laser technologies will make it possible in the near future to increase the reaction yield by four to five orders of magnitude. We note that the possibility of using intense fluxes of neutrons formed in the cleavage mode using laser-accelerated protons for transmutation is also being considered [4, 278].

5.3 Use of gamma sources in solving security problems, nuclear nonproliferation, and combating terrorism

The solution to nuclear security problems was the main topic of the first conference on nuclear photonics [3]. The focus was on the creation of inspection systems for large-capacity containers in order to detect fissile materials. More broadly, controlling the transportation of dangerous or strategically important goods such as explosives and rare and precious metals is important for ensuring national security. Such control can be carried out by scanning the contents of transport containers with gamma radiation.

Currently, the most effective method for identifying fissile materials in containers is believed to be the registration of delayed neutrons produced by a powerful gamma beam [285]. However, a powerful large-area gamma beam is, first, difficult to create, and, second, it is radiation hazardous. Therefore, a two-step scanning procedure has been proposed (Fig. 15). First, a wide low-intensity gamma beam (10^3 photons per second per pixel) irradiates the entire moving container. The size of the pixel as a unit cell of the detector (about 1 cm) is determined by the specified coordinate resolution. The number of pixels depends on the size of the container and the chosen measurement technique. Using the absorption method on a wide beam of a relatively low intensity per unit area, it is possible to determine the presence of high-density substances inside the container. If such an object is detected, repeated irradiation is carried out with a narrow directional high-intensity gamma-ray beam, which is necessary for obtaining a sufficiently large yield of delayed neutrons.

Estimates based of simulation [285] showed that a ^{239}Pu-type object with density $\rho = 19.84$ g cm^{-3}, which is characterized by a minimum delayed neutron yield compared to other actinides (of the order of 6×10^{-3} per fission act), can be detected in a container under the following conditions. A sample with a volume of 1 cm^3 is located in the center of a steel container with a volume of 1 m^3 with a wall thickness of 2 mm. To register 1000 delayed neutrons, it is necessary to create a radiation dose of the order of 10^{10} cm^{-2} with energies from 12 to 16 MeV. Such a dose can be obtained in an electron accelerator with an energy of 16 MeV and a current of

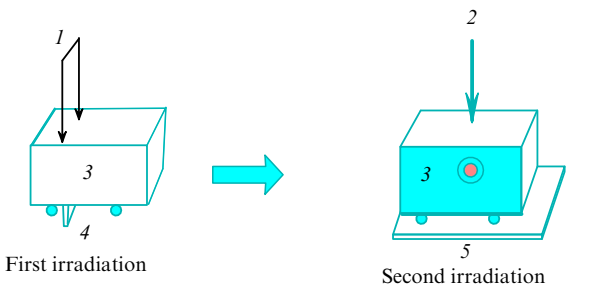

Figure 15. Two-stage method for identifying fissile materials in large-capacity containers: *1*, *2* — beam of bremsstrahlung photons of a linear shape ($E_{max} = 7$ MeV) and a narrow beam ($E_{max} = 25$ MeV), *3* — moving containers, *4* — gamma-detector rack, *5* — detector of delayed neutrons.

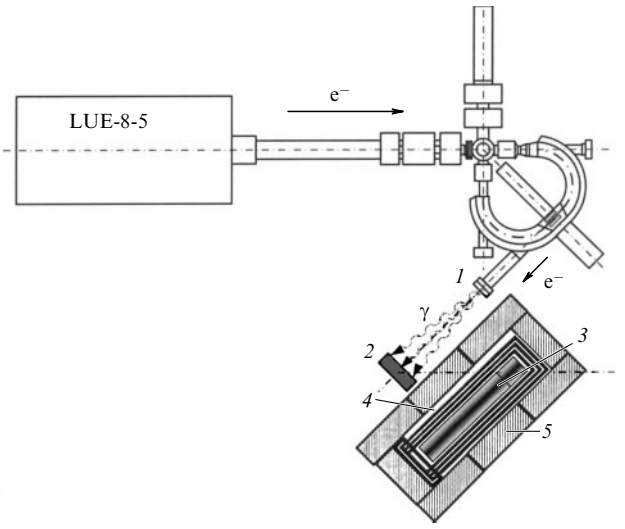

Figure 16. *1* — heater (W); *2* — sample (^{238}U); *3* — detector (stilbene 50 mm (diameter)×50 mm) and PMT; *4*, *5* — protection (three layers of Pb, each 2 mm in thickness, plus 50 mm of Pb).

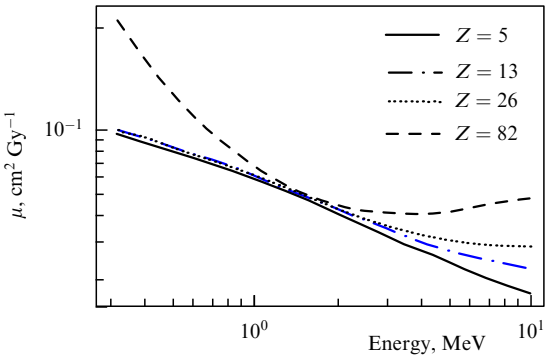

Figure 17. Mass attenuation coefficient for a gamma beam for different materials [286].

100 μA in a time of the order of 1 s when using the converter made of tungsten or tantalum 100 μm in thickness. An optimal detector with a large area (2 × 2 m) with an efficiency of about 30% for detecting neutrons can be created on the basis of a liquid scintillator widely used in neutrino experiments. The transverse size of one pixel is 10 cm^2. A standard silicon photomultiplier tube (PMT) with a cathode area of 10 mm^2 is installed at each pixel to serve as detectors. Estimates show that the optimal measurement time after a 1-second exposure should be 10 s. The experiment on the registration of delayed neutrons performed in [113] using the linear electron accelerator LUE-8-5 showed the reliability of the results obtained in the simulation. Figure 16 shows the schematic of the experiment. To separate neutrons in the background of gamma quanta, the technique of signal separation by pulse shape was used [286].

In modern inspection devices, the so-called dual method [287] is used, in which scanning is performed twice with a bremsstrahlung beam with a different upper edge of the spectrum. The mass attenuation coefficient as a function of the photon energy for different materials is shown in Fig. 17.

Three energy regions can be distinguished in Fig. 17: the initial region where the photoelectric effect dominates and only materials with a large nuclear charge can be separated; the middle one, in which Compton scattering dominates and the materials are practically indistinguishable; and the region where the main effect is exerted by the process of electron–positron pair production and the materials can be distinguished quite well. Among the disadvantages of the dual energy method, we note that it requires scanning at two different beam energies, which leads to complications in the scanner design and the irradiation procedure. An alternative approach was therefore proposed in [288]: to use only one electron beam with an energy of 10 MeV, but to measure not only the spatial but also the energy distribution of the gamma quanta that pass through the container. The simulation results and the first experiments with a bremsstrahlung beam with an energy of 8 MeV [288] showed that the method is promising. A criterion was formulated that distinguishes various materials according to the fraction of the number of photons with energies above 3 MeV. This criterion allows effectively distinguishing materials by their atomic charge.

5.4 Nuclear biology and medicine

Laser-accelerated electrons, the X-ray radiation they generate, and laser-accelerated ions have great potential in biology and medicine, replacing and supplementing methods based on the use of traditional particle accelerators and X-ray generators [289]. Although the average fluxes of particles accelerated by laser radiation are currently much lower than in traditional schemes, it should be taken into account that laser methods are still at an early stage of their development and are in fact rapidly improving. Attention should also be paid to the possibility of accelerating ions of practically any predetermined atom, provided by laser methods, upon a prompt replacement of the target without any need to readjust the rest of the experimental setup.

One of the interesting applications of laser-accelerated ion beams (primarily protons and deuterons) is the production of short-lived isotopes for single-photon emission computed tomography (SPECT) and positron emission tomography (PET) [67]. In most cases, such isotopes are obtained by using beams of fast (10–30 MeV) protons in the reactions $^{100}\mathrm{Mo(p,2n)}^{99m}\mathrm{Tc}$ for SPECT or $^{11}\mathrm{B(p,n)}^{11}\mathrm{C}$, $^{14}\mathrm{N}(\mathrm{p},\alpha)^{11}\mathrm{C}$, $^{18}\mathrm{F(p,n)}^{18}\mathrm{O}$, etc. for PET.

The experimental implementation of such reactions using laser-accelerated protons was first reported in [290–292]. The total number of isotopes was small. In [291], using a laser with a 'high' (10 Hz) pulse repetition rate and energy of 0.8 J for 0.5 h of irradiation in the reaction $^{11}\mathrm{B(p,n)}^{11}\mathrm{C}$ was used to obtain the activity of 13.4 MBq (or 0.3 mCi). With the use of current and upcoming laser systems, we should expect an increase in activity to 10 GBq or more (which already exceeds the therapeutic dose) due to an increase in the repetition rate to 10 kHz and intensity to 4×10^{20} W cm^{-2} [293].

The isotopes used for PET (^{11}C, ^{13}N, ^{15}O, etc.) can be obtained by irradiation not only with protons but also with deuterons. In [294], the activity of 100 Bq was accumulated in 200 s for the ^{11}C isotope (10 Hz, 70 TW). Calculations in [295, 296] show that the activity can significantly exceed 1 GBq for several minutes of irradiation.

There are no experimental studies on the production of the ^{99m}Tc isotope using laser-accelerated protons or heavier ions. This is because the reaction $^{100}\mathrm{Mo(p,2n)}^{99m}\mathrm{Tc}$ requires protons with energies of 10–50 MeV [67]. Calculations show that, when using the ICAN laser system, an activity of 100 GBq can be accumulated in 1 hour. Another possible option for the production of this isotope is to use the reaction $^{100}\mathrm{Mo}(\gamma,\mathrm{n})^{99}\mathrm{Mo}$ in the GDR region (8–14 MeV) of the

gamma beam of a Thomson laser generator [297]. With the photon flux of 10^{13} γ s^{-1} with a maximum energy of 14 MeV, the calculated activity can reach 3 GBq for the optimal irradiation time of 6 h. This gamma flux corresponds to the design parameters of the ELI-NP.

Another promising option for using protons with a relatively low energy, up to 30 MeV, and neutrons generated by them in medicine is therapy based on reactions with stable isotopes of boron, $^{11}B(p)3\alpha$ and $^{11}B(n,\alpha)^7Li$. For the first reaction, protons with an energy of about 1 MeV are sufficient (the cross section maximum is reached at 675 keV [298]). In the second case, epithermal neutrons with energies less than 0.4 eV are needed, which can be obtained by decelerating a beam of fast neutrons [299] coming from reactions like $d(p,n+p)p$, $d(d,n)^3He$ [98], and others. A significant advantage of this technique is the extremely short (about 10 μm) paths of secondary particles, which provide localization of the effect on the cell [300].

Another promising line of research is proton and hadron therapy of tumor tissues (IBT) [301], primarily deep-lying tissues (bone, brain, and so on). The required energies of protons and hadrons in this case are 100–350 MeV per nucleon [302]. The possibility of using laser-accelerated protons to solve these problems was first noted in [303, 304]. Reviews on this topic are given in [66, 305, 306]. In particular, the combination of fast optical control of an ion beam with the concentration of the acting dose in short microbunches can allow irradiating poorly fixed or moving objects [307]. The main restraining factors are the insufficient energy of currently produced ions and the stringent requirements for the monochromaticity and divergence of the beam. In particular, this determines rather categorical conclusions in [308] that laser ion accelerators for IBT have no obvious advantages over traditional accelerators and are not ready to replace them. The significant progress achieved in recent years in the methods and approaches of laser acceleration of ions, nevertheless, allows us to hope for a change in this paradigm. In particular, we note projects such as ELIMED [309, 310] and A-SAIL [311], whose purpose is to develop appropriate technologies and create prototypes of installations for conducting IBT in the near future.

6. Conclusion

The contents of this review suggest that a new scientific discipline, called 'nuclear photonics', has vindicated its right to exist. The point is not only that it has united many interdisciplinary areas but also that it has contributed to the development of new methods for obtaining relativistic particles with energies above nuclear reaction thresholds. Nuclear photonics is primarily associated with the creation of new-generation gamma sources based on the Compton backscattering of laser photons by relativistic electrons. This method allowed obtaining a sufficiently high energy and intensity of a gamma beam, a small angular divergence, and a high degree of polarization. By now, the principal mechanisms of particle acceleration in laser plasma have been established. Laser beams of a high peak power are used to produce stable beams of relativistic electrons, positrons, neutrons, and gamma quanta, which correspond to the problems of nuclear photonics by their characteristics. The main advantage of such sources is their short duration and high peak luminosity.

Great progress has been achieved in the study of nonlinear quantum electrodynamics effects in the interaction of laser radiation with electrons, in particular, in Compton scattering. In the near future, experiments are expected to significantly increase the photon yield (by several orders of magnitude) by controlling the Compton nonlinear scattering process by chirping laser pulses. This will allow creating very compact sources of gamma radiation and significantly expanding the geography of their use.

At present, classical studies of electromagnetic interactions of nuclei are being continued at a higher level. This especially concerns the problem of studying the optical anisotropy of atomic nuclei, first formulated by Baldin in describing the mechanisms of collective excitations of nuclei. The key task is to measure the sum rules connecting the total photoabsorption cross sections of nuclei with the fundamental characteristics of the nucleon, including the anomalous magnetic moment. New experimental data have been obtained on the study of near-threshold photonuclear reactions using real and virtual photons, including information on radiative strength functions.

An important task in nuclear photonics is the study of low-energy isomeric levels near the ground state or a metastable state of the nucleus, which are extremely important for fundamental nuclear physics and in the future can become the basis for a number of dedicated applications (frequency standards, quantum computing, nuclear energy sources, etc.).

An essential factor facilitating the development of nuclear photonics is given by the great amount of applied and interdisciplinary research, including astrophysics, materials science, gamma tomography of large-capacity containers, biology, and medicine. This has become possible thanks to the creation of new-generation gamma sources.

We also note that laser–plasma and traditional accelerator installations do not compete but complement each other. In the first case, pulsed beams of high peak power with a short pulse duration and a relatively low pulse repetition rate are formed, and in the second case, (quasi)continuous beams for conducting coincident experiments.

Acknowledgments. This paper was supported in part by the Russian Foundation for Basic Research in the framework of projects 19-02-00740 and 19-02-00104, and by the Russian Foundation for Basic Research and the State Atomic Energy Corporation Rosatom through research project 20-21-00030.

References

1. Barty C, Pietralla N, Hajima R (Eds) *First Intern. Conf. on Nuclear Photonics, 2016, Monterey, Calif. Abstract Book* (Proc. SPIE, Vol. 10419) (Livermore, Calif.: Lawrence Livermore National Laboratory, 2017) https://doi.org/10.1117/12.2280421
2. Habs D et al. *AIP Conf. Proc.* **1462** 177 (2012)
3. Hayakawa T et al. (Eds) *Nuclear Physics and Gamma-Ray Sources for Nuclear Security and Nonproliferation. Proc. of the Intern. Symp., Ricotti, Tokai-mura, Japan, 28 – 30 January 2014* (Singapore: World Scientific, 2014)
4. Mourou G *Rev. Mod. Phys.* **91** 030501 (2019)
5. Kessel A et al. *Optica* **5** 434 (2018)
6. Danson C N et al. *High Power Laser Sci. Eng.* **7** e64 (2019)
7. Nedorezov V et al. *Phys. Scr.* **94** 015303 (2019)
8. Belyaev V S et al. *Phys. Usp.* **51** 793 (2008); *Usp. Fiz. Nauk* **178** 823 (2008)
9. Dmitrov D et al., in *Proc. 28th European Conf. on Laser-Matter Interaction, Roma, 2004*, p. 591
10. Flegentov V A at al., in *Zababakhinskie Nauchnye Chteniya. Sbornik Materialov Mezhdunarodnoi Konf. 18–22 Marta 2019* (Zababakhin Scientific Readings. Collection of Papers of the Intern. Conf.,

March 18–22, 2019) (Snezhinsk: Izd. RFYAC–VNIITF, 2019) p. 112
11. Korzhimanov A V et al. *Phys. Usp.* **54** 9 (2011); *Usp. Fiz. Nauk* **181** 9 (2011)
12. Mourou G et al. (Eds), ELI – Extreme Light Infrastructure. Whitebook. Science and Technology with Ultra-Intense Lasers. 2011, http://eli-laser.eu/media/1019/eli-whitebook.pdf
13. ELI Beamlines, http://www.eli-beams.eu
14. ELI Nuclear Physics, http://www.eli-np.ro
15. ELI Attosecond, http://www.eli-alps.hu
16. Lozhkarev V V et al. *Laser Phys. Lett.* **4** 421 (2007)
17. Exawatt Center for Extreme Light Studies, https://xcels.iapras.ru/
18. Mourou G et al. *Nat. Photon.* **7** 258 (2013)
19. Tajima T, Dawson J M *Phys. Rev. Lett.* **43** 267 (1979)
20. Pukhov A, Meyer-ter-Vehn J *Appl. Phys. B* **74** 355 (2002)
21. Faure J et al. *Nature* **431** 541 (2004)
22. Geddes C G R et al. *Nature* **431** 538 (2004)
23. Mangles S P D et al. *Nature* **431** 535 (2004)
24. Esarey E et al. *IEEE Trans. Plasma Sci.* **24** 252 (1996)
25. Schlenvoigt H-P et al. ''Laser-based particle acceleration'', in *Advances in Solid State Lasers Development and Applications* (Ed. M Grishin) (Rijeka: InTech, 2010) ID 24
26. Esarey E, Schroeder C B, Leemans W P *Rev. Mod. Phys.* **81** 1229 (2009)
27. Krushelnick K, Malka V *Laser Photon. Rev.* **4** 42 (2010)
28. Lu W et al. *Phys. Rev. ST Accel. Beams* **10** 061301 (2007)
29. Kim H T et al. *Phys. Rev. Lett.* **111** 165002 (2013)
30. Wang X et al. *Nat. Commun.* **4** 1988 (2013)
31. Leemans W P et al. *Phys. Rev. Lett.* **113** 245002 (2014)
32. Gonsalves A J et al. *Phys. Rev. Lett.* **122** 084801 (2019)
33. Faure J et al. *Plasma Phys. Control. Fusion* **61** 014012 (2019)
34. Soloviev A A et al. *Nucl. Instrum. Meth. Phys. Res. A* **653** 35 (2011)
35. Perevalov S E et al. *Plasma Phys. Control. Fusion* **62** 094004 (2020)
36. Kando M et al. *AIP Conf. Proc.* **1024** 197 (2008)
37. Schroeder C B et al. *Phys. Rev. ST Accel. Beams* **13** 101301 (2010)
38. Nakajima K et al. *Phys. Rev. ST Accel. Beams* **14** 091301 (2011)
39. Gizzi L A, in *Laser-Driven Sources High Energy Particles and Radiation. Lecture Notes of the ''Capri'' Advanced Summer School 231* (Springer Proc. in Physics, Vol. 231, Eds L A Gizzi et al.) (Cham: Springer, 2019) p. 1
40. EuPRAXIA, https://www.eupraxia-project.eu/home.html
41. Ferran Pousa A et al. *Phys. Rev. Lett.* **123** 054801 (2019)
42. Tajima T, Nakajima K, Mourou G *Riv. Nuovo Cimento* **40** 33 (2017)
43. Hidding B et al. *Phys. Rev. Lett.* **104** 195002 (2010)
44. Pae K H, Choi I W, Lee J *Phys. Plasmas* **17** 123104 (2010)
45. Masson-Laborde P E et al. *Phys. Plasmas* **21** 123113 (2014)
46. De La Ossa A M et al. *Philos. Trans. R. Soc. A* **377** 2151 (2019)
47. Debus A et al. *Phys. Rev. X* **9** 031044 (2019)
48. Palastro J P et al. *Phys. Rev. Lett.* **124** 134802 (2020)
49. Kruer W L, Estabrook K *Phys. Fluids* **28** 430 (1985)
50. Pukhov A, Sheng Z-M, Meyer-ter-Vehn J *Phys. Plasmas* **6** 2847 (1999)
51. Rax J M *Phys. Fluids B* **4** 3962 (1992)
52. Sheng Z-M et al. *Phys. Rev. Lett.* **88** 055004 (2002)
53. Gordon D et al. *Phys. Rev. Lett.* **80** 2133 (1998)
54. Tsymbalov I N et al. *Quantum Electron.* **49** 386 (2019); *Kvantovaya Elektron.* **49** 386 (2019)
55. Macchi A *A Superintense Laser-Plasma Interaction Theory Primer* (New York: Springer, 2013)
56. Gibbon P *Short Pulse Laser Interactions with Matter: an Introduction* (London: Imperial College Press, 2005)
57. Beg F N et al. *Phys. Plasmas* **4** 447 (1997)
58. Compant La Fontaine A *J. Phys. D* **47** 325201 (2014)
59. Key M H et al. *Phys. Plasmas* **5** 1966 (1998)
60. Ma Y et al. *Proc. Natl. Acad. Sci. USA* **115** 6980 (2018)
61. Tsymbalov I et al. *Plasma Phys. Control. Fusion* **61** 075016 (2019)
62. Compant La Fontaine A et al. *Phys. Plasmas* **26** 113109 (2019)
63. Macchi A et al. *Plasma Phys. Control. Fusion* **56** 039501 (2014)
64. Macchi A, Borghesi M, Passoni M *Rev. Mod. Phys.* **85** 751 (2013)
65. Daido H, Nishiuchi M, Pirozhkov A S *Rep. Prog. Phys.* **75** 056401 (2012)
66. Bulanov S V et al. *Phys. Usp.* **57** 1149 (2014); *Usp. Fiz. Nauk* **184** 1265 (2014)
67. Bychenkov V Yu et al. *Phys. Usp.* **58** 71 (2015); *Usp. Fiz. Nauk* **185** 77 (2015)
68. Wilks S C et al. *Phys. Plasmas* **8** 542 (2001)
69. Schreiber J et al. *Phys. Rev. Lett.* **97** 045005 (2006)
70. Snavely R A et al. *Phys. Rev. Lett.* **85** 2945 (2000)
71. Clark E L et al. *Phys. Rev. Lett.* **84** 670 (2000)
72. Maksimchuk A et al. *Phys. Rev. Lett.* **84** 4108 (2000)
73. Wagner F et al. *Phys. Rev. Lett.* **116** 205002 (2016)
74. Toncian T et al. *Science* **312** 410 (2006)
75. Clark E L et al. *Phys. Rev. Lett.* **85** 1654 (2000)
76. Hegelich B M et al. *Phys. Plasmas* **12** 056314 (2005)
77. Volkov R V et al. *Quantum Electron.* **33** 981 (2003); *Kvantovaya Elektron.* **33** 981 (2003)
78. Gordienko V M et al. *Appl. Phys. B* **80** 733 (2005)
79. Hegelich B M et al. *Nature* **439** 441 (2006)
80. Schwoerer H et al. *Nature* **439** 445 (2006)
81. Tayyab M et al. *Phys. Plasmas* **25** 123102 (2018)
82. Esirkepov T et al. *Phys. Rev. Lett.* **92** 175003 (2004)
83. Martins S F et al. *Astrophys. J* **695** L189 (2009)
84. Yin L et al. *Phys. Plasmas* **14** 056706 (2007)
85. Jung D et al. *Phys. Plasmas* **20** 083103 (2013)
86. Nishiuchi M et al. *Phys. Plasmas* **22** 033107 (2015)
87. Petrov G M et al. *Phys. Plasmas* **23** 063108 (2016)
88. Sharma A, Kamperidis C *Sci. Rep.* **9** 13840 (2019)
89. Rykovanov S G et al. *New J. Phys.* **10** 113005 (2008)
90. Bulanov S V et al. *Phys. Rev. Lett.* **104** 135003 (2010)
91. Tamburini M et al. *Phys. Rev. E* **85** 016407 (2012)
92. Badziak J *J. Phys. Conf. Ser.* **959** 012001 (2018)
93. Bychenkov V Y, Tikhonchuk V T, Tolokonnikov S V *J. Exp. Theor. Phys.* **88** 1137 (1999); *Zh. Eksp. Teor. Fiz.* **115** 2080 (1999)
94. Ledingham K W D, Galster W *New J. Phys.* **12** 045005 (2010)
95. Alvarez J et al. *Phys. Procedia* **60** 29 (2014)
96. Bolton P R, Parodi K, Schreiber J *Applications of Laser-Driven Particle Acceleration* (Boca Raton, Fl.: CRC Press, Taylor and Francis Group, 2018)
97. Roth M et al. *Phys. Rev. Lett.* **110** 044802 (2013)
98. Kar S et al. *New J. Phys.* **18** 053002 (2016)
99. Chen S N et al. *Matter Radiat. Extremes* **4** 054402 (2019)
100. Mirfayzi S R et al. *Appl. Phys. Lett.* **111** 044101 (2017)
101. Di Piazza A et al. *Rev. Mod. Phys.* **84** 1177 (2012)
102. Chen H et al. *Phys. Rev. Lett.* **105** 015003 (2010)
103. Chen H et al. *Phys. Plasmas* **20** 013111 (2013)
104. Liang E et al. *Sci. Rep.* **5** 13968 (2015)
105. Xu T et al. *Phys. Plasmas* **23** 033109 (2016)
106. Ecklund S D, in *Workshop on Intense Positron Beams, Idaho Falls, ID, USA, 18–19 June 1987* (Eds W P Kells, E H Ottewitte) (Singapore: World Scientific, 1988) p. 42; SLAC-PUB-4437
107. Gorlova D A et al. *Quantum Electron.* **47** 522 (2017); *Kvantovaya Elektron.* **47** 522 (2017)
108. Nedorezov V G, Turinge A A, Shatunov Yu M *Phys. Usp.* **47** 341 (2004); *Usp. Fiz. Nauk* **174** 353 (2004)
109. Sun C, Wu Y K *Phys. Rev. ST Accel. Beams* **14** 044701 (2011)
110. Rykovanov S G et al. *J. Phys. B* **47** 234013 (2014)
111. Krafft G A, Priebe G *Rev. Accel. Sci. Technol.* **03** 147 (2010)
112. Hajima R *Phys. Procedia* **84** 35 (2016)
113. Nedorezov V G, Savel'ev-Trofimov A B *Phys. At. Nucl.* **80** 1477 (2017); Translated from Russian: *Yad. Fiz. Inzhiniring* **7** 479 (2016)
114. Ur C A *AIP Conf. Proc.* **1645** 237 (2015)
115. Corde S et al. *Rev. Mod. Phys.* **85** 1 (2013)
116. Schwoerer H et al. *Phys. Rev. Lett.* **96** 014802 (2006)
117. Ta Phuoc K et al. *Nat. Photon.* **6** 308 (2012)
118. Tsai H E et al. *AIP Conf. Proc.* **1777** 080006 (2016)
119. Yu C et al. *Sci. Rep.* **6** 29518 (2016)
120. Chen S et al. *Phys. Rev. Lett.* **110** 155003 (2013)
121. Powers N D et al. *Nat. Photon.* **8** 28(2014)
122. Liu C et al. *Opt. Lett.* **39** 4132 (2014)
123. Rykovanov S G et al. *J. Phys. B* **47** 234013 (2014)
124. Geddes C G et al. *Nucl. Instrum. Meth. Phys. Res. B* **350** 116 (2015)
125. Geddes C G et al. *AIP Conf. Proc.* **1777** 110002 (2016)
126. Leemans W ''Laser technology for k-BELLA and beyond'', Technical Report (Berkeley, CA: Lawrence Berkeley National Laboratory, 2017)
127. Hartemann F V et al. *Phys. Rev. Lett.* **105** 130801 (2010)

128. Sarachik E S, Schappert G T *Phys. Rev. D* **1** 2738 (1970)
129. Alferov D F et al. *Part. Accel.* **9** 223 (1979)
130. Clarke J *The Science and Technology of Undulators and Wigglers* (Oxford: Oxford Univ. Press, 2004)
131. Berestetskii V, Lifshitz E M, Pitaevskii L P *Quantum Electrodynamics* (Oxford: Oxford Univ. Press, 1982); Translated from Russian: *Kvantovaya Elektrodinamika* (Moscow: Fizmatlit, 2004)
132. Wolkow D M *Z. Phys.* **94** 250 (1935)
133. Di Piazza A et al. *Rev. Mod. Phys.* **84** 1177 (2012)
134. Nikishov A I, Ritus V I *Sov. Phys. JETP* **20** 757 (1965); *Zh. Eksp. Teor. Fiz.* **47** 1130 (1964)
135. Esarey E, Ride S K, Sprangle P *Phys. Rev. E* **48** 3003 (1993)
136. Hartemann F V et al. *Phys. Rev. E* **54** 2956 (1996)
137. Heinzl T, Seipt D, Kämpfer B *Phys. Rev. A* **81** 022125 (2010)
138. Brau C A *Phys. Rev. ST Accel. Beams* **7** 020701 (2004)
139. Seipt D, Kämpfer B *Phys. Rev. A* **83** 022101 (2011)
140. Kharin V Yu, Seipt D, Rykovanov S G *Phys. Rev. A* **93** 063801 (2016)
141. Seipt D et al. *J. Plasma Phys.* **82** 655820203 (2016)
142. Krajewska K, Kamiński J Z *Phys. Rev. A* **85** 062102 (2012)
143. Krajewska K, Twardy M, Kamiński J Z *Phys. Rev. A* **89** 052123 (2014)
144. Krafft G A *Phys. Rev. Lett.* **92** 204802 (2004)
145. Mackenroth F, Di Piazza A *Phys. Rev. A* **83** 032106 (2011)
146. Boca M, Florescu V *Phys. Rev. A* **80** 053403 (2009)
147. Narozhnyi N B, Fofanov M S *J. Exp. Theor. Phys.* **83** 14 (1996); *Zh. Eksp. Teor. Fiz.* **110** 26 (1996)
148. Ruijter M, Kharin V Y, Rykovanov S G *J. Phys. B* **51** 225701 (2018)
149. Maroli C et al. *Phys. Rev. ST Accel. Beams* **16** 030706 (2013)
150. Englert T J, Rinehart E A *Phys. Rev. A* **28** 1539 (1983)
151. Babzien M et al. *Phys. Rev. Lett.* **96** 054802 (2006)
152. Sakai Y et al. *Phys. Rev. ST Accel. Beams* **18** 060702 (2015)
153. Sakai Y et al. *Phys. Rev. Accel. Beams* **20** 060701 (2017)
154. Chen S, Maksimchuk A, Umstadter D *Nature* **396** 653 (1998)
155. Bula C et al. *Phys. Rev. Lett.* **76** 3116 (1996)
156. Sarri G et al. *Phys. Rev. Lett.* **113** 224801 (2014)
157. Khrennikov K et al. *Phys. Rev. Lett.* **114** 195003 (2015)
158. Yan W et al. *Nat. Photon.* **11** 514 (2017)
159. Cole J M et al. *Phys. Rev. X* **8** 11020 (2018)
160. Hartemann F V et al. *Phys. Rev. Lett.* **105** 130801 (2010)
161. Ghebregziabher I, Shadwick B A, Umstadter D *Phys. Rev. ST Accel. Beams* **16** 030705 (2013)
162. Terzić B et al. *Phys. Rev. Lett.* **112** 074801 (2014)
163. Rykovanov S G et al. *Phys. Rev. Accel. Beams* **19** 030701 (2016)
164. Terzić B, Reeves C, Krafft G A *Phys. Rev. Accel. Beams* **19** 044403 (2016)
165. Maroli C et al. *J. Appl. Phys.* **124** 063105 (2018)
166. Seipt D et al. *Phys. Rev. A* **91** 033402 (2015)
167. Seipt D, Kharin V Yu, Rykovanov S G *Phys. Rev. Lett.* **122** 204802 (2019)
168. Kharin V Yu, Seipt D, Rykovanov S G *Phys. Rev. Lett.* **120** 044802 (2018)
169. Baldin A *Nucl. Phys.* **18** 310 (1960)
170. Torresand J, Torner L (Eds) *Twisted Photons*: *Applications of Light with Orbital Angular Momentum* (Weinheim: Wiley-VCH, 2011)
171. Wang J W, Zepf M, Rykovanov S G *Nat. Commun.* **10** 5554 (2019)
172. Gorchtein M et al. *Phys. Rev. C* **70** 055202 (2004)
173. Gerasimov S *Phys. Lett.* **5** 259 (1963)
174. Drell S D, Hearn A C *Phys. Rev. Lett.* **16** 908 (1966)
175. Gell-Mann M, Goldberger M L *Phys. Rev.* **96** 1433 (1954)
176. Gurevich G et al. *Nucl. Phys. A* **273** 326 (1976)
177. Eisenberg J M, Greiner W *Nuclear Theory* Vol. 1 *Nuclear Models-Collective and Single Particle Phenomena* (Amsterdam: North-Holland Pub. Co., 1975); Translated into Russian: *Modeli Yader*: *Kollektivnye i Odnochastichnye Yavleniya* (Moscow: Atomizdat, 1975)
178. Kanada-En'yo Y, Shikata Y *Phys. Rev. C* **95** 064319 (2017)
179. Soloviev V G *Theory of Complex Nuclei* (Oxford: Pergamon Press, 1976); Translated into Russian: *Teoriya Slozhnykh Yader* (Moscow: Nauka, 1971)
180. Kamerdzhiev S P et al. *Phys. At. Nucl.* **82** 366 (2019); *Yad. Fiz.* **82** 320 (2019)
181. Özel-Tashenov B et al. *Phys. Rev. C* **90** 024304 (2014)
182. Govaert K et al. *Phys. Rev. C* **57** 2229 (1998)
183. Weller H R, Ahmed M W, Wu Y K *Nucl. Phys. News* **25** (3) 19 (2015)
184. Levinger J S *Nuclear Photo-Disintegration* (London: Oxford Univ. Press, 1960); Translated into Russian: *Fotoyadernye Reaktsii* (Moscow.: IL, 1962)
185. Ahrens J et al. *Nucl. Phys. A* **251** 479 (1975)
186. Kazakov A A et al. *JETP Lett.* **40** 1271 (1984); *Zh. Eksp. Teor Fiz.* **40** 445 (1984)
187. Sanabria J C et al. *Phys. Rev. C* **61** 034604 (2000)
188. Muccifora V et al. *Phys. Rev. C* **60** 064616 (1999)
189. Nedorezov V G, Ranyuk Yu N *Fotodelenie Yader za Gigantskim Rezonansom* (Photofission of Nuclei Behind Giant Resonance) (Kiev: Naukova Dumka, 1989)
190. Fermi E *Z. Phys.* **29** 315 (1924)
191. Weizsacker C *Z. Phys.* **29** 612 (1934)
192. Williams E J *Phys. Rev.* **45** 729 (1934)
193. Barber W, Wiedling T *Nucl. Phys.* **18** 575 (1960)
194. Volynec E et al. *Nucl. Phys. A* **224** 205 (1975)
195. Polikanov S M *Izometriya Formy Atomnykh Yader* (Isomerism of the Shape of Atomic Nuclei) (Moscow: Atomizdat, 1977)
196. Nedorezov V G, Polikanov S M *Fiz. Elem. Chast. Atom. Yad.* **8** 374 (1977)
197. Norreys P A et al. *Phys. Plasmas* **6** 2150 (1999)
198. Ledingham K W D et al. *Phys. Rev. Lett.* **84** 899 (2000)
199. Cowan T E et al. *Phys. Rev. Lett.* **84** 903 (2000)
200. Spencer I et al. *Rev. Sci. Instrum.* **73** 3801 (2002)
201. Belyaev V S et al. *Laser Phys. 7***21** 1398 (2011)
202. Spohr K M et al. *New J. Phys.* **10** 043037 (2008)
203. Tsymbalov I N et al. *Phys. Atom. Nucl.* **80** 397 (2017); *Yad. Fiz.* **80** 189 (2017)
204. Ericson T, Weise W *Pions and Nuclei* (Oxford: Clarendon Press, 1988); Translated into Russian: *Piony i Yadra* (Moscow: Nauka, 1991) s. 335
205. Tsymbalov I et al. *Plasma Phys. Control. Fusion* **63** (2) 022001 (2021)
206. Nedorezov V G, Savel'ev-Trofimov A B *Yad. Fiz. Inzhiniring* **7** 479 (2016)
207. Andreev A V, Gordienko V M, Savel'ev A B *Quantum Electron.* **31** 941 (2001); *Kvantovaya Elektron.* **31** 941 (2001)
208. Karamian S A *Phys. Part. Nucl.* **39** 490 (2008); *Fiz. Elem. Chast. Atom. Yad.* **39** 951 (2008)
209. Tkalya E V *Phys. Usp.* **48** 525 (2005); *Usp. Fiz. Nauk* **175** 555 (2005)
210. Okamoto K, in *Laser Interaction and Related Plasma Phenomena* Vol. 4A (Eds H J Schwarz, H Hora) (Boston, Mass.: Springer, 1977) p. 283
211. Letokhov V S *Sov. Phys. JETP* **37** 787 (1973); *Zh. Eksp. Teor. Fiz.* **64** 1555 (1973)
212. Andreev A *Vestn. Mosk. Gos. Univ. Ser. 3. Fiz. Astron.* **35** 28 (1994)
213. Oganessian Y, Karamian S *Laser Phys.* **2** 336 (1995)
214. Tkalya E V *Phys. Rev. Lett.* **106** 162501 (2011)
215. Peik E, Tamm C *Europhys. Lett.* **61** 181 (2003)
216. Campbell C J et al. *Phys. Rev. Lett.* **108** 120802 (2012)
217. Kazakov G A et al. *New J. Phys.* **14** 083019 (2012)
218. von der Wense L, Seiferle B, Thirolf P G *Meas. Tech.* **60** 1178 (2018)
219. Gunst J, Keitel C H, Pálffy A *Sci. Rep.* **6** 25136 (2016)
220. Cohen R L, Miller G L, West K W *Phys. Rev. Lett.* **41** 381 (1978)
221. Gerdau E, DeWaard H *Hyperfine Interact.* **123–124** 847 (1999)
222. Pálffy A, Evers J, Keitel C H *Phys. Rev. C* **77** 044602 (2008)
223. Gunst J et al. *Phys. Rev. Lett.* **112** 082501 (2014)
224. Méot V et al. *Phys. Rev. C* **75** 064306 (2007)
225. Helmer R G, Reich C W *Phys. Rev. C* **49** 1845 (1994)
226. Tkalya E V et al. *Phys. Scr.* **53** 296 (1996)
227. Thielking J et al. *Nature* **556** 321 (2018)
228. Seiferle B et al. *Nature* **573** 243 (2019)
229. Seiferle B, von der Wense L, Thirolf P G *Phys. Rev. Lett.* **118** 042501 (2017)
230. Harston M R, Chemin J F *Phys. Rev. C* **59** 2462 (1999)
231. Andreev A V et al. *J. Exp. Theor. Phys.* **91** 1163 (2000); *Zh. Eksp. Teor. Fiz.* **118** 1343 (2000)
232. Chutko OV et al. *Laser Phys.* **13** 190 (2003)
233. Stewart J C, Pyatt, Kedar D J *Astrophys. J.* **144** 1203 (1966)
234. Andreev A V et al. *JETP Lett.* **66** 331 (1997); *Pis'ma Zh. Eksp. Teor. Fiz.* **66** 312 (1997)
235. Claverie G et al. *Phys. Rev. C* **70** 044303 (2004)

236. Golovin G V et al. *Quantum Electron.* **41** 222 (2011); *Kvantovaya Elektron.* **41** 222 (2011)
237. Savel'ev A et al. *Plasma Phys. Control. Fusion* **59** 035004 (2017)
238. Denis-Petit D et al. *Phys. Rev. C* **96** 024604 (2017)
239. Gunst J et al. *Phys. Plasmas* **22** 112706 (2015)
240. Pálffy A, Evers J, Keitel C H *Phys. Rev. Lett.* **99** 172502 (2007)
241. Wu Y et al. *Phys. Rev. Lett.* **120** 052504 (2018)
242. Gunst J et al. *Phys. Rev. E* **97** 063205 (2018)
243. Vinko S M et al. *Nature* **482** 59 (2012)
244. Colgan J et al. *Phys. Rev. Lett.* **110** 125001 (2013)
245. Pikuz S A (Jr.) et al. *Phys. Usp.* **57** 702 (2014); *Usp. Fiz. Nauk* **184** 759 (2014)
246. von der Wense L et al. *Eur. Phys. J. A* **56** 176 (2020)
247. Borisyuk P V et al. *Phys. Rev. C* **100** 044306 (2019)
248. von der Wense L et al. *Phys. Rev. Lett.* **119** 132503 (2017)
249. Masuda T et al. *Nature* **573** 238 (2019)
250. Allaria E et al. *Nat. Photon.* **6** 699 (2012)
251. Saule T et al. *Nat. Commun.* **10** 458 (2019)
252. Krausz F, Ivanov M *Rev. Mod. Phys.* **81** 163 (2009)
253. Corkum P B *Phys. Rev. Lett.* **71** 1994 (1993)
254. Kornev A S, Zon B A *Laser Phys. Lett.* **4** 588 (2007)
255. Ganeev R A *Phys. Usp.* **56** 772 (2013); *Usp. Fiz. Nauk* **183** 815 (2013)
256. Strelkov V V et al. *Phys. Usp.* **59** 425 (2016); *Usp. Fiz. Nauk* **186** 449 (2016)
257. Andreev A V et al. *Phys. Rev. A* **99** 013422 (2019)
258. Horowitz C J, Piekarewicz J, in *Proc. of the Intern. Symp., Electromagnetic Interactions in Nuclear and Hadron Physics, Osaka, Japan, 4–7 December 2001* (Eds M Fujiwara, T Shima) (Singapore: World Scientific, 2002) p. 63
259. Austin S M, in *Proc. of the Intern. Symp., Electromagnetic Interactions in Nuclear and Hadron Physics, Osaka, Japan, 4–7 December 2001* (Eds M Fujiwara, T Shima) (Singapore: World Scientific, 2002) p. 73
260. Utsunomiya H et al., in *Proc. of the Intern. Symp., Electromagnetic Interactions in Nuclear and Hadron Physics, Osaka, Japan, 4–7 December 2001* (Eds M Fujiwara, T Shima) (Singapore: World Scientific, 2002) p. 83
261. Mohr P et al., in *Proc. of the Intern. Symp., Electromagnetic Interactions in Nuclear and Hadron Physics, Osaka, Japan, 4–7 December 2001* (Eds M Fujiwara, T Shima) (Singapore: World Scientific, 2002) p. 207
262. Langanke K et al. *Phys. Rev. Lett.* **93** 202501 (2004)
263. Gurzadyan V G et al. *Mod. Phys. Lett. A* **20** 491 (2005)
264. Spergel D N et al. *Astrophys. J. Suppl.* **170** 377 (2007)
265. Bocquet J P et al. *Nucl. Phys. A* **622** c124 (1997)
266. Nedorezov V G "Photonuclear reactions: astrophysics implications", in *Proc. LV National Conf. on Nuclear Physics. Frontiers in the Physics of Nucleus, 2005* (St. Petersburg: St. Petersburg State Univ., 2005)
267. Karnaukhov V A, Petrov L A *Yadra, Udalennye ot Linii Beta-stabil'nosti* (Nuclei Further from the Beta Stability Line) (Moscow: Energoizdat, 1981)
268. Remington B A et al. *Science* **284** 1488 (1999)
269. Belyaev V S et al. *Phys. Atom. Nucl.* **79** 648 (2016); *Yad. Fiz.* **79** 438 (2016)
270. Ishkhanov B S, Kapitonov I M, Tutyn' I A *Nukleosintez vo Vselennoi* (Nucleosynthesis in the Universe) (Moscow: Librokom, 2017)
271. Ratzel U et al. *Phys. Rev. C* **70** 065803 (2004)
272. Wallerstein G et al. *Rev. Mod. Phys.* **69** 995 (1997)
273. Cowan J J, Cameron A G W, Truran J W *Astrophys. J.* **294** 656 (1985)
274. Diamond H et al. *Phys. Rev.* **119** 2000 (1960)
275. Comsan M N H "Spallation neutron sources for science and technology", in *Proc. of the 8th Conf. on Nuclear and Particle Physics, 20–24 Nov. 2011, Hurghada, Egypt*
276. Pomerantz I et al. *Phys. Rev. Lett.* **113** 184801 (2014)
277. Higginson D P et al. *Phys. Rev. Lett.* **115** 054802 (2015)
278. Galés S "Nuclear energy and waste transmutation with high power accelerator and laser systems", https://indico.cern.ch/event/617648/contributions/2517094/attachments/1442136/2220662/18_GALES_IZES Talk-Nuclear-Transmutation-040417.pdf
279. MYRRHA, https://myrrha.be/
280. Ledingham K W D et al. *J. Phys. D* **36** L79 (2003)
281. Irani E, Omidvar H, Sadighi-Bonabi R *Energy Conversion Management* **77** 558 (2014)
282. Wang X-L et al. *Laser Part. Beams* **34** 433 (2016)
283. Wang X L et al. *Phys. Plasmas* **24** 093105 (2017)
284. Rehman H U, Lee J, Kim Y *Int. J. Energy Res.* **42** 236 (2018)
285. Dzhilavyan L Z et al. *Phys. Part. Nucl.* **50** 626 (2019); *Fiz. Elem. Chast. Atom. Yad.* **50** 637 (2019)
286. Zelenaya A et al. *Phys. Part. Nucl.* **50** 581 (2019); *Fiz. Elem. Chast. At. Yad.* **50** 680 (2019)
287. Verbitsky S S et al. *Instrum. Exp. Tech.* **55** 174 (2012); *Prib. Tekh. Eksp.* (2) 30 (2012)
288. Spirin D, Berdnikov Y, Gavrish Y *Sci. Tech. Statements St. Petersburg State Polytech. Univ. Phys. Math.* **2** 98 (2010)
289. Giulietti A (Ed.) *Laser-Driven Particle Acceleration Towards Radiobiology and Medicine* (Cham: Springer Intern. Publ., 2016)
290. Zepf M et al. *Phys. Plasmas* **8** 2323 (2001)
291. Fritzler S et al. *Appl. Phys. Lett.* **83** 3039 (2003)
292. Ledingham K W D et al. *J. Phys. D* **37** 2341 (2004)
293. Lefebvre E et al. *J. Appl. Phys.* **100** 113308 (2006)
294. Fujimoto M et al. *Rev. Sci. Instrum.* **80** 113301 (2009)
295. Kimura S, Bonasera A *Nucl. Instrum. Meth. Phys. Res. A* **637** 164 (2011)
296. Maksimchuk A et al. *Appl. Phys. Lett.* **102** 191117 (2013)
297. Lee J, Rehman H ur, Kim Y *Nucl. Technol.* **201** 41 (2018)
298. Sikora M H, Weller H R *J. Fusion Energy* **35** 538 (2016)
299. Kasesaz Y, Rahmani F, Khalafi H *Appl. Radiat. Isot.* **103** 173 (2015)
300. Cirrone G A P et al. *Sci. Rep.* **8** 1141 (2018)
301. Schardt D, Elsässer T, Schulz-Ertner D *Rev. Mod. Phys.* **82** 383 (2010)
302. Borghesi M, Macchi A "Laser-driven ion accelerators: state of the art and applications", in *Laser-Driven Particle Acceleration Towards Radiobiology and Medicine* (Ed. A Giulietti) (Cham: Springer Intern. Publ., 2016) p. 221
303. Bulanov S et al. *Phys. Lett. A* **299** 240 (2002)
304. Bulanov S V, Khoroshkov V S *Plasma Phys. Rep.* **28** 453 (2002); *Fiz. Plazmy* **28** 493 (2002)
305. Aurand B et al. *Phys. Plasmas* **23** 023113 (2016)
306. Karsch L et al. *Acta Oncol.* **56** 1359 (2017)
307. Hofmann K M, Schell S, Wilkens J J *J. Biophoton.* **5** 903 (2012)
308. Linz U, Alonso J *Phys. Rev. Accel. Beams* **19** 124802 (2016)
309. ELIMAIA-ELIMED installed at ELI Beamlines, https://www.eli-beams.eu/news-and-events/media-news-and-events/elimaia-elimed-installed-at-eli-beamlines/
310. Schillaci F et al. *J. Phys. Conf. Ser.* **508** 012010 (2014)
311. A-SAIL Project, https://www.qub.ac.uk/research-centres/A-SAILProject
312. Ginzburg V et al. *Opt. Express* **29** 28297 (2021)